Supporting Information

AggFluor: Fluorogenic Toolbox Enables Direct Visualization of the Multi-Step Protein Aggregation Process in Live Cells

Charles H. Wolstenholme[1], Hang Hu[4,5], Songtao Ye[1], Brian E. Funk[1], Divya Jain[1], Chia-Heng Hsiung[2], Gang Ning[3], Yu Liu*[1,6], Xiaosong Li*[4], Xin Zhang*[1,2,3]

[1]Department of Chemistry, [2]Department of Biochemistry and Molecular Biology, [3]The Huck Institute of Life Sciences, The Pennsylvania State University, University Park, Pennsylvania 16802, United States, [4]Department of Chemistry, [5]Molecular Engineering and Sciences Institute, University of Washington, Seattle, Washington 98105, United States, [6]Dalian Institute of Chemical Physics, 457 Zhongshan Road, Dalian 116023, China

Corresponding Authors: Xin Zhang (xuz31@psu.edu), Xiaosong Li (xsli@uw.edu), Yu Liu (liuyu@dicp.ac.cn).

Contents

1. Experimental methods

1.1 Viscosity Sensitivity Measurements.

From 2 mM probe stock solutions in DMSO, all probes were prepared as 5 μM, 25 ºC in a series of ethylene glycol/glycerol (EG/G) solutions in the following mixing ratios: EG/G = 70/30 (81 cP), 50/50 (183 cP), 40/60 (283 cP), 30/70 (426 cP), 20/80 (621 cP), 0/100 (1069 cp). All samples were placed on a Vortex-Genie 2 for at least 15 minutes to thoroughly mix before transferring to a 96-well clear flat bottom polystyrene plate (Costar) for spectral measurements. Fluorescent measurements were initially carried out on each dye dissolved in 100% glycerol to determine wavelength of maximal excitation and emission peaks. Subsequently, emission intensity at the peak wavelength was used to record fluorescence intensity for each probe in EG/G mixtures as defined above. Six independent measurements were conducted to produce an average value for each data. Logarithm plot of emission intensity as a function of viscosity was used to determine the value of viscosity sensitivity (x) based on the Förster-Hoffmann equation $logI = xlog\eta + A$, wherein η is viscosity (cP), I is the fluorescence intensity, x is the viscosity sensitivity.

1.2 Absorbance, Spectra, Fluorescence Spectra.

Absorbance, excitation and emission spectra were recorded using a Tecan M1000Pro fluorescence plate reader from 10 μM probe solutions in glycerol, 25ºC. After thorough mixing, 100 μL sample aliquots were transferred to a 96-well clear flat bottom polystyrene plate (Costar).

1.3 Quantum Yield and Brightness.

Quantum yield measurements were carried out following established protocol [1]. P1 (Φ_{std} = 0.22, 100% glycerol, 25 ºC) was used as the reference standard. Probes were diluted independently from a 2 mM stock solution in DMSO to produce samples (1–5 μM in 1 μM increments) in 100% glycerol, 25 ºC for analysis. Emission spectra were recorded with excitation at wavelengths that overlap with the P1 absorption standard. The integrals of the resulting emission spectra were plotted as a function of the absorbances at the excitation wavelength for each sample. Quantum yields were calculated from the obtained data according to **Equation 1**, where gradient corresponds to the linear slope of the relationship between absorbance and emission integral and η is the refractive index of the solvent. Standard error of this gradient is reported as percent of the

slope for all quantum yields, example gradient for compound 1 shown below. Absorbance maxima for each sample were plotted as a function of concentration to obtain the respective molar extinction coefficient (ε) via the slope of the resulting linear curve. Brightness was calculated to be Φ × ε.

Equation 1: $$\Phi_x = \frac{\text{Gradient}_x}{\text{Gradient}_{std}} \bullet \frac{\eta_x^2}{\eta_{std}^2} \bullet \Phi_{std}$$

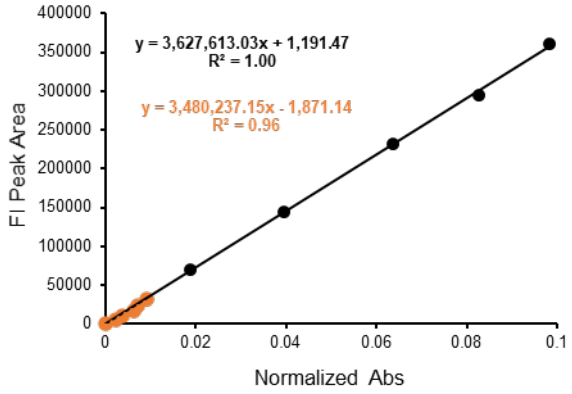

1.4 Purification of Recombinant POI-Halo Proteins.

SOD1(A4V)-Halo-His6 plasmid was constructed from the SOD1(WT)-Halo-His6 using the QuickChange PCR to introduce point mutations of A4V, G85R or G93A. Fluc(R188Q) was acquired as a gift from Ulric Hartl (Addgene Plasmid # 90171). This gene was sub-cloned into a pET29b vector containing Halo-6His to generate the Fluc(R188Q)-Halo-His6 plasmid.

Plasmids were transformed into E. coli BL21DE3* competent cells harboring a pBAD vector encoding σ32-I54N [2]. A single colony was picked and inoculated into 5 mL LB containing ampicillin and kanamycin, followed by serial dilution. The cultures were grown overnight at 37˚C with shaking at 200 rpm. Once OD_{600} reached ~0.8, 15 mL of starter culture was introduced into a 1.5 L LB media supplemented with ampicillin and kanamycin. When OD_{600} reached ~0.4, L-arabinose was added to a final concentration of 0.2 mg/ml to induce the expression of σ32-I54N that could globally upregulate cellular chaperones to assist folding of recombinant proteins. Subsequently, the cultured was subjected to 30 ºC for further growth. When OD_{600} reached ~0.8, isopropyl -D-1-thiogalactopyranoside was added to a final concentration of 0.5 mM to induce the expression of recombinant protein. Expression was carried out overnight at 18 ˚C. Cells were harvested and stored in a -80˚C freezer until use.

To carry out protein purification, cells were thawed and lysed by sonication on ice in Buffer A (50 mM Tris-HCl, pH 7.5, 100 mM NaCl) with addition of 1mM phenylmethyl sulfonyl fluoride (PMSF). The lysate was cleared by centrifugation at 16,000 G for 60 min at 4˚C. Supernatant was collected and loaded onto a 6 mL pre-charged IMAC Ni^{2+} column (ProfinityTM IMAC Resin, Bio-Rad), followed by a washing step with Buffer A. SOD1 or FLUC was then eluted with gradient addition of Buffer B (50 mM Tris-HCl, pH 7.5, 100 mM NaCl, 500 mM imidazole). Fractions were identified by SDS-PAGE analyses, pooled and loaded onto a gel filtration column (HiPrepTM 16/60 SephacrylTM S200HR, GE Healthcare) to allow further purification and buffer exchange (50 mM Tris-HCl, pH 7.5, 100 mM NaCl). The resulted protein fractions were analyzed by SDS-PAGE to have >95% purity before concentrated and flash frozen.

1.5 In Vitro Aggregation Assays of SOD1-Halo and Fluc-Halo.

SOD1(mutants)-Halo: Aggregation was carried out with DPBS buffer with 80 mM EDTA added after conjugation to chelate the structural metal. Conjugation of P1h or P18h to purified SOD1-Halo protein was completed by incubation of the probe (5 μM) with protein (25 μM) in a 1.5 mL microcentrifuge tube for 15 min in the absence of ambient light prior. Reaction was carried out quiescently at indicated temperatures. Fluorescence of P1h was measured at E_x = 530 nm/E_m = 620 nm and P18h E_x = 450 nm/E_m = 510 nm using a Tecan M1000Pro fluorescence plate reader.

Fluc-R118Q-Halo: Aggregation was carried out with DPBS buffer. Conjugation of P1h or P18h to purified Fluc-Halo protein was completed by incubation of the probe (5 μM) with protein (25 μM) in a 1.5 mL microcentrifuge tube for 15 min at 4˚C in the absence of ambient light prior. Reaction was carried out quiescently at indicated temperatures. Fluorescence of P1h was measured at E_x = 530 nm/E_m = 620 nm and P18h E_x = 450 nm/E_m = 510 nm using a Tecan M1000Pro fluorescence plate reader.

1.6 Negative Staining Electron Microscopy.

Before applying for sample, Formvar films with carbon-coated 400 mesh EM grids were plasma-discharged. A small amount of sample (~5 μL) was loaded into the grid. The grids were cleaned to remove excess of the sample, stained with 1% aqueous uranyl and then imaged.

1.7 Confocal Fluorescence Microscopy.

HEK293T cells were seeded at approximately 25% confluency in poly-D-lysine coated 35 mm glass bottom dishes. For 24 hrs, cells were grown in DMEM media supplemented with 10% FBS and Penicillin-Streptomycin antibiotics until they reached 40-50% confluency. Transfection was carried out using X-tremeGene™ 9 DNA transfection reagent according to the manufacturer's instructions. To label SOD1-Halo and Htt-Halo proteins, protein expression was carried out in the presence of 0.5 μM P1h, 0.5 μM P18h and/or 0.5 μM Coumarin Halo-Tag ligand to form covalent conjugate with the Halo-Tag. To remove unbound Halo ligands, the cells were washed by replacing media with fresh DMEM supplemented with 0.1 μg/mL Hoechst 33342 (no Hoechst 33342 was added if the Coumarin Halo-Tag ligand was used) and incubating for 30 min at 37 °C. Confocal images were obtained using Olympus FluoView™ FV1000 or Zeiss LSM 880 confocal microscope. P1h was visualized using the green laser (543/563 nm). P18h was visualized using the blue (453/458 nm) laser. Nuclear staining and coumarin Halo-Tag ligand were visualized using the violet laser (405 nm). For all imaging experiments, laser intensities, gain and other settings were kept identical to exclude artifacts and ensure robustness of data.

1.8 Small molecule Induced Aggregation, Disaggregation and Degradation.

MG132: POI-Halo was transiently transfected and expressed in HEK293T cells for 24 h (SOD1(mutant)-Halo) or 48 h (Htt-Q46-Halo), in the presence fluorescent ligands as indicated. Subsequently, excess probes were washed away by incubating cells with fresh DMEM media for 30 min at 37 ºC. Then, cells were replaced into fresh DMEM media containing 5 μM MG132 to induce proteome aggregation. Cells were treated for 8 or 24 h prior to fluorescence confocal microscopy.

Hsp70 activator YM-1: Htt-Q110-Halo was transiently transfected in HEK293T cells in the presence of indicated fluorescent ligands. After 30 min, YM-1 was added to a final concentration of 1 μM. Proteins were expressed for 48 h, and subsequently excess probes were washed away by incubating cells with fresh DMEM media for 30 min at 37 ºC.

Proteasome activator PD169316: Htt-Q46-Halo or Htt-Q110-Halo were transiently transfected in HEK293T cells in the presence of indicated fluorescent ligands. After 30 min, PD169316 was added to a final concentration of 1 μM. Proteins were expressed for 48 h, and subsequently excess probes were washed away by incubating cells with fresh DMEM media for 30 min at 37 ºC.

Co-treatment using YM-1 and PD169316: Htt-Q110-Halo were transiently transfected in HEK293T cells in the presence of indicated fluorescent ligands. After 30 min, YM-1 and PD169316 were added to a final concentration of 1 μM for each compound. Proteins were expressed for 48 h, and subsequently excess probes were washed away by incubating cells with fresh DMEM media for 30 min at 37 ºC.

1.9 PES of the Rotational Motion Along the φ Dihedral Angle Using CASSCF Rigid Scan

Computational analyses were carried out to study potential energy surface (PES) of the rotational motion along the φ dihedral angle for AggFluor P1 and P18 at both the ground (S_0) and excited (S_1) state. To obtain accurate descriptions of electronic states across the PES of the bond rotation, the multi-reference nature of the broken bond near the twisted geometry must be addressed [3]. Thus, in this work, state-averaged complete active space self-consistent field (CASSCF) method was used to construct the PES of the rotational motion along the φ dihedral angle [4-8]. Bases set was chosen to be 6-31G(d,p) [9]. All the calculations are performed in Gaussian computational package version 16 A.03.

The initial ground state geometries of both P1 and P18 were optimized in gas phase at the level of B3LYP with 6-31G(d,p) [10]. The optimized geometries are verified as true minima via frequency calculations. To perform rigid scans, the φ dihedral angle was rotated from planar (0º) to perpendicular (90º) geometry with an interval of 15º, while all other degrees of freedom were frozen. Then, single-point CASSCF calculations were conducted at each geometry to plot the PES. Particularly, CASSCF calculation are state-averaged over the ground state (S_0) and first excited state (S_1) with equal weights. The choices of CAS for P1 and P18 are CAS(10,10) and CAS(6,6), respectively. After state-averaged CASSCF optimizations, the molecular orbitals in active space share similar characters between P1 and P18. Population analysis including Mulliken Charges was performed using state-averaged CASSCF wave functions.

1.10 In Vitro Tubridy Assays of SOD1-Halo and Fluc-Halo

SOD1(mutants)-Halo: Aggregation of protein (25 μM) was carried out with DPBS buffer with 80 mM EDTA added to chelate the structural metal. 250μL of protein was added to a quartz cuvette and reaction was carried out quiescently at 59˚C. Light scattering was monitored over 1h via absorbance at 395nm using a temperature-controlled Agilent Technologies Carry 300 Series UV-Vis Spectrophotometer.

Fluc-R118Q-Halo: Aggregation of protein (25 μM) was carried out with DPBS buffer. 250μL of protein was added to a quartz cuvette and reaction was carried out quiescently at 57˚C. Light scattering was monitored over 1h via absorbance at 395nm using a temperature-controlled Agilent Technologies Carry 300 Series UV-Vis Spectrophotometer.

2. Supplementary Tables

Table S1: Photophysical properties of AggFluor P1-P18, P1h, P18h.

Compound	λ_{max} (nm)	Em. (nm)	Φ (927 cP)	Φ* ($3 \cdot 10^{11}$ cP)	ε	B	χ	Stoke's Shift (nm)
P1 (P1h)	540	632	0.22	0.33	36,195	7,963	0.28	92
P2	524	604	0.21	0.52	1,878	357	0.32	80
P3	526	612	0.26	0.69	14,109	3,668	0.36	86
P4	520	609	0.20	0.57	8,671	1,734	0.38	89
P5	519	608	0.19	0.67	12,071	2,293	0.41	89
P6	522	649	0.23	0.90	5,353	1,231	0.43	127
P7	536	655	0.24	1.00	8,616	2,068	0.51	119
P8	545	596	0.20	0.33	3,818	764	0.26	51
P9	525	616	0.22	0.43	12,920	2,842	0.31	91
P10	515	602	0.20	0.36	9,762	1,952	0.39	87
P11	520	619	0.18	0.80	11,382	2,049	0.49	99
P12	524	600	0.19	0.84	17,218	3,271	0.50	76
P13	512	598	0.16	0.23	3,778	604	0.30	86
P14	481	577	0.11	0.52	3,127	344	0.43	96
P15	473	574	0.05	0.27	755	38	0.47	101
P16	514	599	0.15	0.98	6,275	941	0.48	85
P17	511	592	0.15	0.97	10,895	1,634	0.53	81
P18 (P18h)	450	518	0.03	0.36	23,717	949	0.68	68

*Quantum yield at $3 \cdot 10^{11}$ cP was extrapolated using fold change of fluorescent intensity

Table S2: The optimized geometry of P1 at the ground state (S_0). The total energy at this geometry is −1186.40684958 Hartree. The geometry was optimized using Gaussian computational package version 16 A.03.

Atom Label	Atom	X(Å)	Y(Å)	Z(Å)
1	C	-0.03778000	0.93963000	-1.03151200
2	C	2.09609600	1.33176400	-1.00771800
3	C	1.44830100	2.60027500	-1.43765800
4	N	0.08674800	2.27556600	-1.42997200
5	N	1.11884100	0.36728500	-0.77943400
6	O	1.91806800	3.69337400	-1.73909500
7	C	3.45173700	1.22244900	-0.88278100
8	H	3.99160900	2.13638600	-1.12532100
9	C	-1.33533100	0.30770600	-0.92634200
10	H	-2.19708800	0.92181900	-1.16873700
11	C	-1.49118800	-0.98549000	-0.54682100
12	H	-0.58016000	-1.53744400	-0.32267100
13	C	4.26167200	0.09567400	-0.48458100
14	C	5.66555800	0.24476600	-0.43319100
15	C	3.74281100	-1.17149500	-0.12851800
16	C	6.50814100	-0.79107600	-0.05852100
17	H	6.10262500	1.20614000	-0.69213400
18	C	4.57373900	-2.21537100	0.24732600
19	H	2.66936800	-1.31833100	-0.14970500
20	C	5.98490700	-2.06325400	0.28520000
21	H	7.57532600	-0.60941800	-0.03346700
22	H	4.12045000	-3.16179500	0.51547700
23	N	6.81441300	-3.11393700	0.63484000
24	C	6.24149900	-4.34860000	1.14942000
25	H	5.69015100	-4.19752900	2.09034400
26	H	5.55741500	-4.79941200	0.42164800
27	H	7.04407400	-5.06383000	1.33422300
28	C	8.23702200	-2.87755600	0.82775500
29	H	8.69828100	-2.48284700	-0.08465500
30	H	8.43952700	-2.17089000	1.64745000
31	H	8.72734300	-3.82324400	1.06231400

32	C	-2.73186500	-1.72827300	-0.40351500
33	C	-2.68627800	-3.07897400	-0.00338600
34	C	-4.01352600	-1.18452100	-0.63464600
35	C	-3.83190500	-3.84786800	0.15410400
36	H	-1.71972100	-3.53635700	0.19326200
37	C	-5.16868900	-1.93516200	-0.48337100
38	H	-4.11481800	-0.14616900	-0.93612600
39	C	-5.11449300	-3.29969500	-0.09257100
40	H	-3.72555700	-4.87800500	0.47008500
41	H	-6.12260600	-1.45782800	-0.66994700
42	N	-6.26344900	-4.05858400	0.03367400
43	C	-7.56805700	-3.42004800	-0.05757000
44	H	-7.70184900	-2.93092100	-1.02921300
45	H	-8.34413700	-4.18038900	0.03738500
46	H	-7.72478600	-2.66757800	0.73048700
47	C	-6.18349500	-5.40099300	0.58940200
48	H	-5.52298300	-6.03729500	-0.01068300
49	H	-5.81516800	-5.40583600	1.62686600
50	H	-7.17635200	-5.85212000	0.57689600
51	C	-0.95791200	3.21474400	-1.78682300
52	H	-1.52795400	2.86723800	-2.65509200
53	H	-1.64311400	3.38697200	-0.94989200
54	H	-0.46361700	4.15509300	-2.04002700

Table S3: The optimized geometry of P1 at the excited state (S_1). The total energy at this geometry is −1186.32262097 Hartree. The geometry was optimized using Gaussian computational package version 16 A.03.

Atom Label	Atom	X(Å)	Y(Å)	Z(Å)
1	C	-0.07818300	1.02860100	-1.06644500
2	C	2.07895700	1.38135400	-1.01026800
3	C	1.43933000	2.66076700	-1.45462400
4	N	0.07957600	2.35415000	-1.46417400
5	N	1.12281800	0.44343700	-0.79392600
6	O	1.93615100	3.74234700	-1.75058300
7	C	3.45902300	1.28542200	-0.87404600
8	H	4.00429600	2.19490300	-1.11326200
9	C	-1.33031600	0.39744000	-0.96621900
10	H	-2.21220900	0.97805500	-1.21290100
11	C	-1.43800200	-0.93443200	-0.56198100
12	H	-0.50337400	-1.44233200	-0.33674700
13	C	4.22286900	0.14903200	-0.46257400
14	C	5.64036700	0.24705100	-0.38192700
15	C	3.65186900	-1.11082100	-0.11694000
16	C	6.43328900	-0.81368400	0.00931300
17	H	6.11406000	1.19136500	-0.63766400
18	C	4.43900000	-2.17837000	0.27586200
19	H	2.57492400	-1.21859000	-0.16809300
20	C	5.85441600	-2.06890900	0.35336000
21	H	7.50673800	-0.67535900	0.05051000
22	H	3.95114400	-3.11248200	0.52709200
23	N	6.63720100	-3.13277400	0.74545200
24	C	6.02469300	-4.40719300	1.09074400
25	H	5.33237700	-4.30581800	1.93718000
26	H	5.46892800	-4.83067800	0.24343900
27	H	6.80429600	-5.11474300	1.37291400
28	C	8.08459300	-2.99618300	0.81606600
29	H	8.51549200	-2.74619500	-0.16270800
30	H	8.38258500	-2.21725000	1.53055200
31	H	8.51786200	-3.94060300	1.14519000

32	C	-2.63397800	-1.69567800	-0.41424700
33	C	-2.56641500	-3.05249700	0.00850600
34	C	-3.94273700	-1.18826200	-0.65826500
35	C	-3.69121200	-3.84013800	0.16993200
36	H	-1.59019400	-3.48389100	0.21707600
37	C	-5.07546300	-1.96836900	-0.49949200
38	H	-4.07004800	-0.15710800	-0.97276000
39	C	-4.99105900	-3.32591500	-0.09081100
40	H	-3.56294000	-4.86335400	0.50123400
41	H	-6.04088100	-1.51761400	-0.69537500
42	N	-6.12309600	-4.11914600	0.03308200
43	C	-7.44044200	-3.50634900	-0.03626900
44	H	-7.58525300	-2.99519400	-0.99422300
45	H	-8.20046500	-4.28542800	0.03884100
46	H	-7.61112300	-2.77605700	0.77132000
47	C	-6.01663900	-5.42958700	0.65532200
48	H	-5.31117000	-6.06641500	0.11068700
49	H	-5.68830800	-5.37465700	1.70600700
50	H	-6.99144800	-5.91856800	0.62535800
51	C	-0.95513300	3.29887400	-1.83427000
52	H	-1.51749200	2.94180600	-2.70331700
53	H	-1.64710600	3.46605400	-1.00225700
54	H	-0.46032400	4.23873000	-2.08621000

Table S4: Potential energy surface (PES) of P1 at both S_0 and S_1 states as a function of the φ angle using SA-CASSCF. Plot of the PES is shown in **Figure 2e**.

	Energy Raw (A.U.)		Energy relative to S_0 (eV)	
Dihedral Angle φ	S_0	S_1	S_0	S_1
0	-1178.85699	-1178.706589	0	4.092561611
15	-1178.853035	-1178.703802	0.107619505	4.168398668
30	-1178.841752	-1178.695365	0.414641218	4.397977875
45	-1178.841513	-1178.693456	0.421144647	4.449923674
60	-1178.831856	-1178.6942	0.683921274	4.42967869
70	-1178.809217	-1178.700269	1.299951103	4.264535131
80	-1178.793322	-1178.707498	1.732469948	4.067826812
90	-1178.779813	-1178.715317	2.100063347	3.855064003

Table S5: Mulliken Charges Analysis of P1 at both S_0 and S_1 states as a function of the φ angle.

Dihedral Angle	CSF |1> Coefficients		CSF |2> Coefficients		Q_EDG		Q_EWG		Q_EDG – Q_EWG	
φ	S_0	S_1	S_0	S_1	S_0	S_1	S_0	S_1	S_0	S_1
0	0.89421	-0.26304	0.25742	0.88530	0.18834	0.18446	-0.18834	-0.18446	0.37668	0.36892
15	0.89417	0.26197	-0.25671	0.88607	0.19678	0.18167	-0.19678	-0.18167	0.39357	0.36334
30	0.89954	0.23381	-0.23043	0.89581	0.21869	0.16746	-0.21869	-0.16745	0.43738	0.33491
45	0.77457	0.51613	-0.50107	0.76426	0.15742	0.56475	-0.15742	-0.56475	0.31483	1.12950
60	0.64646	0.67251	0.66039	-0.63484	0.14433	0.65590	-0.14433	-0.65590	0.28866	1.31179
70	0.52431	0.77190	-0.75990	0.51493	0.11073	0.73147	-0.11073	-0.73147	0.22146	1.46294
80	0.32248	0.87599	-0.86314	0.31710	0.04363	0.82488	-0.04363	-0.82488	0.08727	1.64975
90	0.00000	0.93351	-0.92009	0.00000	-0.00857	0.88368	0.00857	-0.88367	-0.01713	1.76735

Table S6: The optimized geometry of P18 at the ground state (S_0). The total energy at this geometry is − 783.268427396 Hartree. The geometry was optimized using Gaussian computational package version 16 A.03.

Atom Label	Atom	X(Å)	Y(Å)	Z(Å)
1	C	-1.30584500	-1.00916000	1.39520800
2	C	0.12134900	-1.07072400	-0.23240000
3	C	-1.16637300	-1.54696800	-0.79720700
4	N	-2.03443900	-1.47991600	0.30568700
5	N	-0.05562700	-0.76056700	1.12596400
6	O	-1.47814000	-1.92090200	-1.92315200
7	C	1.25545200	-0.97732700	-0.98141100
8	H	1.12384900	-1.28269600	-2.01861700
9	C	2.58378600	-0.54314100	-0.61613200
10	C	3.59621500	-0.54195700	-1.60084200
11	C	2.95106900	-0.10588400	0.67835800
12	C	4.89436300	-0.13826700	-1.32821400
13	H	3.35065300	-0.86516500	-2.60957600
14	C	4.24446400	0.29995100	0.96483000
15	H	2.19728900	-0.08819700	1.45684600
16	C	5.26175600	0.28925700	-0.02671800
17	H	5.62340700	-0.15520800	-2.12857100
18	H	4.46862500	0.63012800	1.97164200
19	N	6.55516600	0.67372700	0.26610500
20	C	6.86940000	1.23953200	1.56977200
21	H	6.32393300	2.17552000	1.76225500
22	H	6.63326300	0.53461200	2.37543200
23	H	7.93809700	1.45132100	1.61822000
24	C	7.54020300	0.77922300	-0.79973600
25	H	7.67376100	-0.18082100	-1.31209200
26	H	7.26399900	1.53358500	-1.55184600
27	H	8.50209600	1.06170200	-0.37051000
28	C	-1.93757100	-0.82059600	2.73337300
29	H	-2.76667800	-0.10443000	2.68593100
30	H	-2.34171400	-1.76375500	3.12028900
31	H	-1.18511700	-0.44602400	3.42840500

32	C	-3.43494000	-1.85183300	0.25194500
33	H	-4.08275800	-1.00406200	0.49856100
34	H	-3.63985800	-2.16963700	-0.77256900
35	H	-3.65426300	-2.68093600	0.93293300

Table S7: The optimized geometry of P18 at the excited state (S_1). The total energy at this geometry is − 783.155254054 Hartree. The geometry was optimized using Gaussian computational package version 16 A.03.

Atom Label	Atom	X(Å)	Y(Å)	Z(Å)
1	C	-1.31185400	-1.00684100	1.39420500
2	C	0.11133300	-1.07342600	-0.25807100
3	C	-1.16937500	-1.55523200	-0.79249400
4	N	-2.03440100	-1.48288700	0.33072400
5	N	-0.03643600	-0.75690000	1.06863000
6	O	-1.50316400	-1.94464400	-1.91636400
7	C	1.26752800	-0.98274500	-1.06015400
8	H	1.12190800	-1.29770600	-2.09030200
9	C	2.56898000	-0.53777300	-0.68608600
10	C	3.61539000	-0.52168600	-1.65785600
11	C	2.91860600	-0.09189600	0.62930500
12	C	4.89560500	-0.10193800	-1.35901600
13	H	3.39213200	-0.85270600	-2.66879400
14	C	4.20191700	0.32995700	0.93252000
15	H	2.15119400	-0.09015500	1.39434900
16	C	5.23270100	0.34084600	-0.04529800
17	H	5.64410700	-0.11409300	-2.14196000
18	H	4.40950800	0.65665200	1.94460600
19	N	6.51364200	0.76315200	0.25904800
20	C	6.83670000	1.20900200	1.60416200
21	H	6.22756600	2.07483900	1.89889400
22	H	6.67364300	0.41234200	2.34349400
23	H	7.88593000	1.50137300	1.64415800
24	C	7.55205300	0.76137200	-0.75851300
25	H	7.73237600	-0.24893400	-1.15131100
26	H	7.29163800	1.41367000	-1.60351700
27	H	8.48196500	1.12653400	-0.32275700
28	C	-1.88745300	-0.79620700	2.74783600
29	H	-2.71739500	-0.07525500	2.73597500
30	H	-2.28012400	-1.72814600	3.17913700
31	H	-1.10414000	-0.41300700	3.40425400

32	C	-3.43197200	-1.86357700	0.28826400
33	H	-4.08015700	-1.01572400	0.53443600
34	H	-3.64208300	-2.19269600	-0.73164900
35	H	-3.63899300	-2.68518100	0.98230700

Table S8: Potential energy surface (PES) of P18 at both S_0 and S_1 states as a function of the φ angle using SA-CASSCF. Plot of the PES is shown in **Figure 4e**.

	Energy Raw (A.U.)		Energy relative to S_0 (eV)	
Dihedral Angle φ	S_0	S_1	S_0	S_1
0	-778.3427395	-778.1600738	0	4.970516363
15	-778.3383638	-778.1585174	0.119067173	5.012867563
30	-778.3236779	-778.1569341	0.518685198	5.055950739
45	-778.3037824	-778.1589319	1.060061648	5.001588604
60	-778.2797177	-778.167343	1.7148862	4.772714162
70	-778.2626953	-778.1761654	2.178082726	4.532647835
80	-778.2478885	-778.1855009	2.580990561	4.278619545
90	-778.2411303	-778.190128	2.764887941	4.152711527

Table S9: Mulliken charges analysis of P18 at both S_0 and S_1 states as a function of the φ angle.

Dihedral Angle	CSF |1> Coefficients		CSF |2> Coefficients		Q_EDG		Q_EWG		Q_EDG - Q_EWG	
φ	S_0	S_1	S_0	S_1	S_0	S_1	S_0	S_1	S_0	S_1
0	0.93920	0.03230	0.07114	-0.85117	0.15329	0.26822	-0.15329	-0.26822	0.30659	0.53644
15	0.93821	0.02769	0.06718	-0.86217	0.15844	0.28811	-0.15843	-0.28811	0.31687	0.57622
30	0.92654	0.18736	0.15659	-0.90953	0.16803	0.46876	-0.16803	-0.46876	0.33606	0.93752
45	0.80462	0.52606	0.50967	-0.79030	0.17636	0.56502	-0.17636	-0.56502	0.35273	1.13003
60	0.67799	0.68591	0.67392	-0.66411	0.16497	0.63691	-0.16497	-0.63691	0.32995	1.27382
70	0.56074	0.78513	0.77329	-0.54988	0.13112	0.70670	-0.13112	-0.70670	0.26224	1.41340
80	0.35642	0.89700	0.88405	-0.35015	0.05730	0.80448	-0.05730	-0.80448	0.11460	1.60895
90	0.00000	0.96528	0.95150	0.00547	-0.00676	0.87547	0.00676	-0.87547	-0.01352	1.75094

3. Supplementary Figures

3.1 Figures 1-20: Spectra of AggFluor P1-P18, P1h, P18h

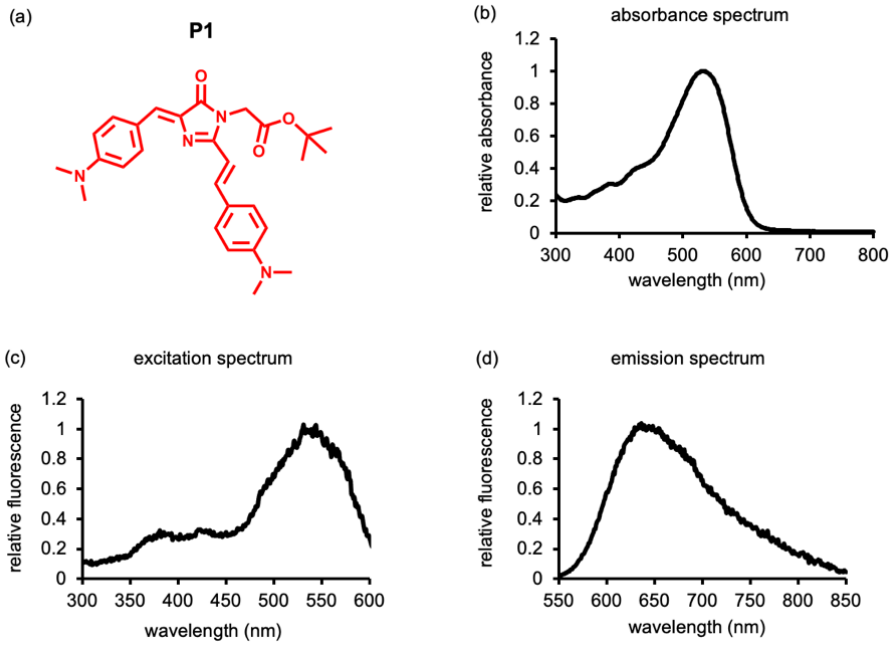

Figure S1: a) Structure of AggFluor P1. **b**) Normalized absorbance spectrum. **c**) Normalized excitation spectrum. **d**) Normalized emission spectrum. All spectra were collected using 10 μM compound in 100% glycerol, 25ºC.

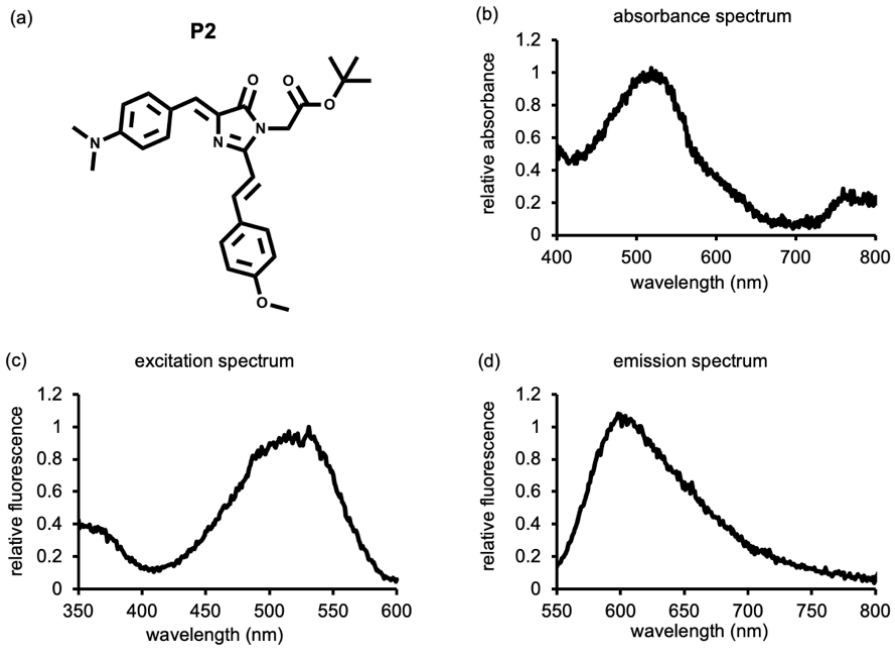

Figure S2: a) Structure of AggFluor P2. **b**) Normalized absorbance spectrum. **c**) Normalized excitation spectrum. **d**) Normalized emission spectrum. All spectra were collected using 10 μM compound in 100% glycerol, 25ºC.

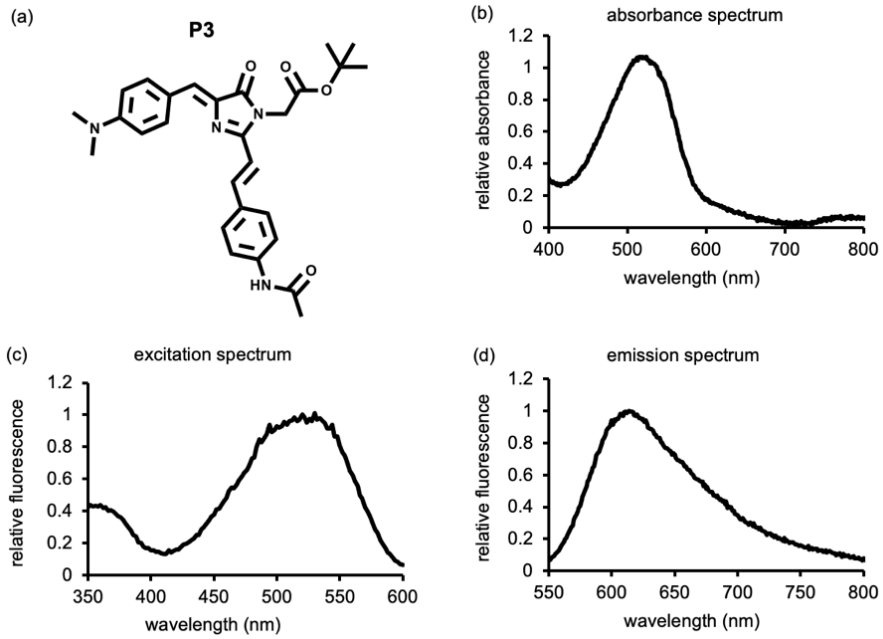

Figure S3: a) Structure of AggFluor P3. **b**) Normalized absorbance spectrum. **c**) Normalized excitation spectrum. **d**) Normalized emission spectrum. All spectra were collected using 10 μM compound in 100% glycerol, 25ºC.

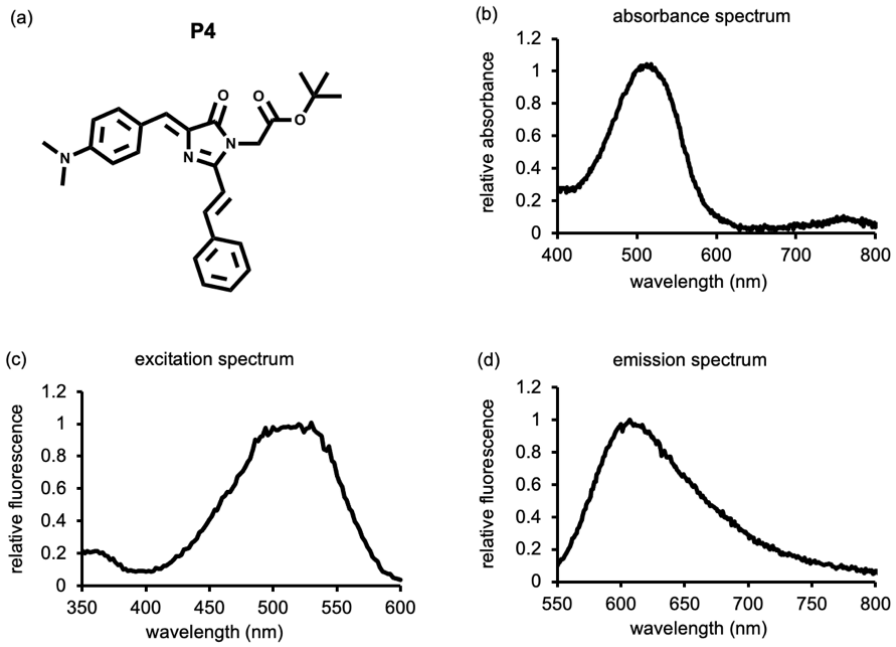

Figure S4: a) Structure of AggFluor P4. **b**) Normalized absorbance spectrum. **c**) Normalized excitation spectrum. **d**) Normalized emission spectrum. All spectra were collected using 10 μM compound in 100% glycerol, 25ºC.

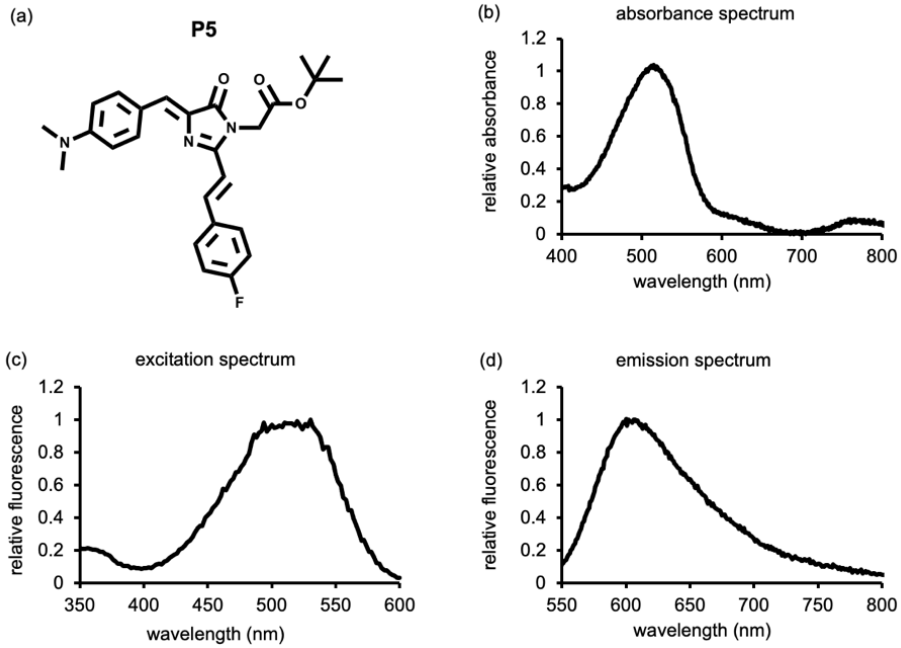

Figure S5: a) Structure of AggFluor P5. **b**) Normalized absorbance spectrum. **c**) Normalized excitation spectrum. **d**) Normalized emission spectrum. All spectra were collected using 10 μM compound in 100% glycerol, 25ºC.

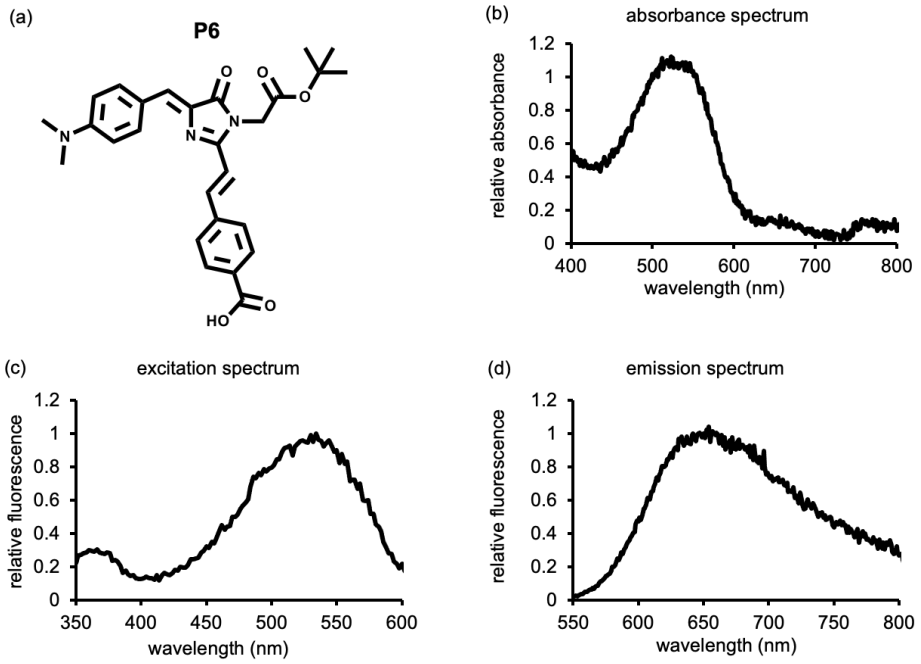

Figure S6: a) Structure of AggFluor P6. **b**) Normalized absorbance spectrum. **c**) Normalized excitation spectrum. **d**) Normalized emission spectrum. All spectra were collected using 10 μM compound in 100% glycerol, 25ºC.

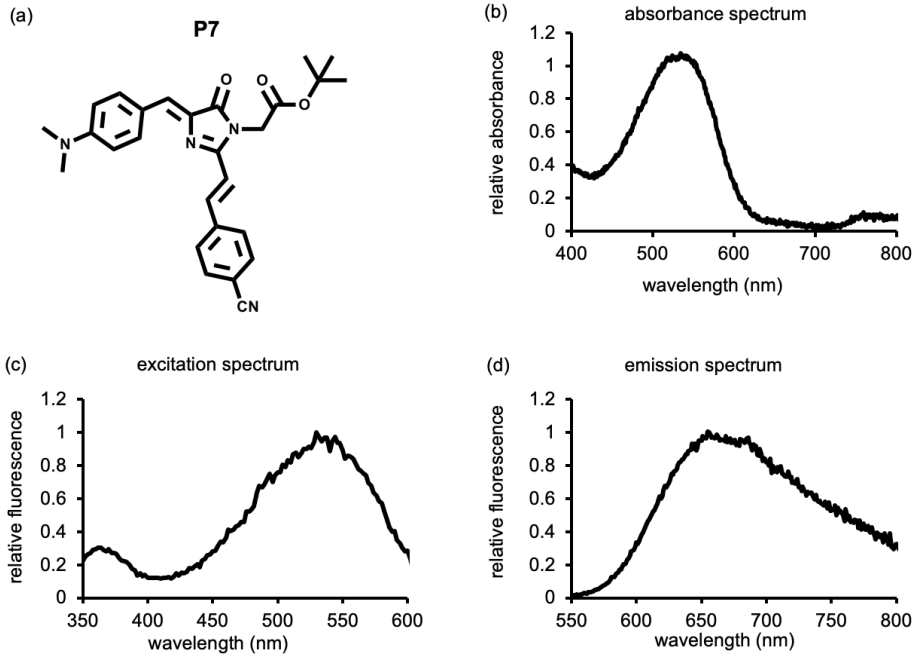

Figure S7: a) Structure of AggFluor P7. **b**) Normalized absorbance spectrum. **c**) Normalized excitation spectrum. **d**) Normalized emission spectrum. All spectra were collected using 10 μM compound in 100% glycerol, 25ºC.

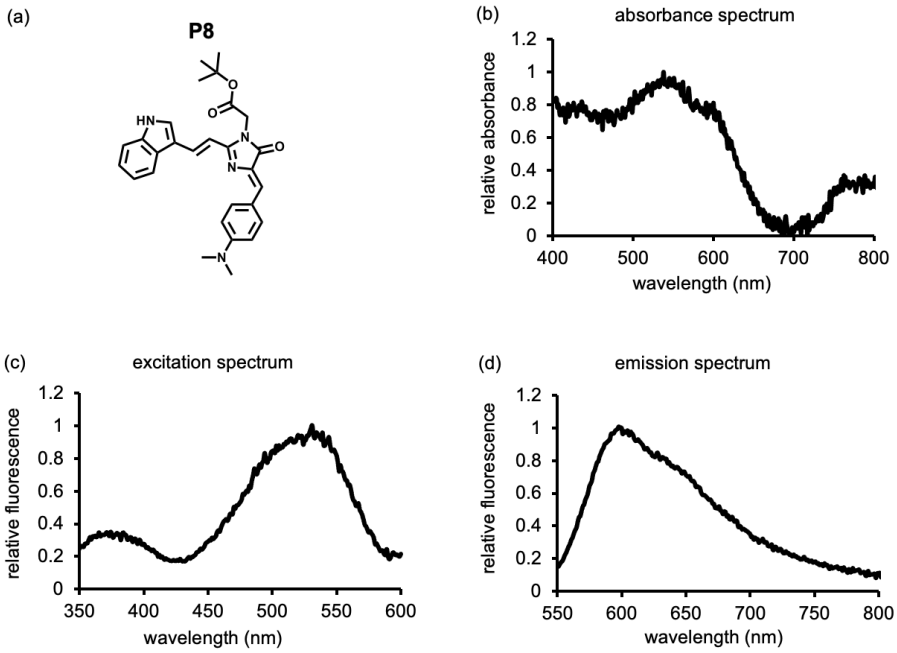

Figure S8: a) Structure of AggFluor P8. **b**) Normalized absorbance spectrum. **c**) Normalized excitation spectrum. **d**) Normalized emission spectrum. All spectra were collected using 10 μM compound in 100% glycerol, 25ºC.

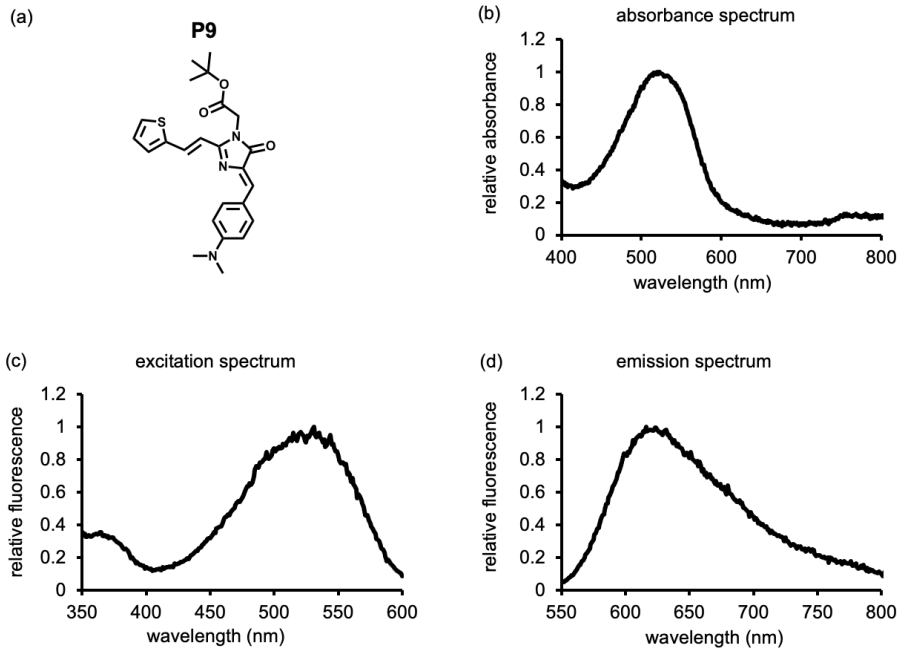

Figure S9: a) Structure of AggFluor P9. **b**) Normalized absorbance spectrum. **c**) Normalized excitation spectrum. **d**) Normalized emission spectrum. All spectra were collected using 10 μM compound in 100% glycerol, 25ºC.

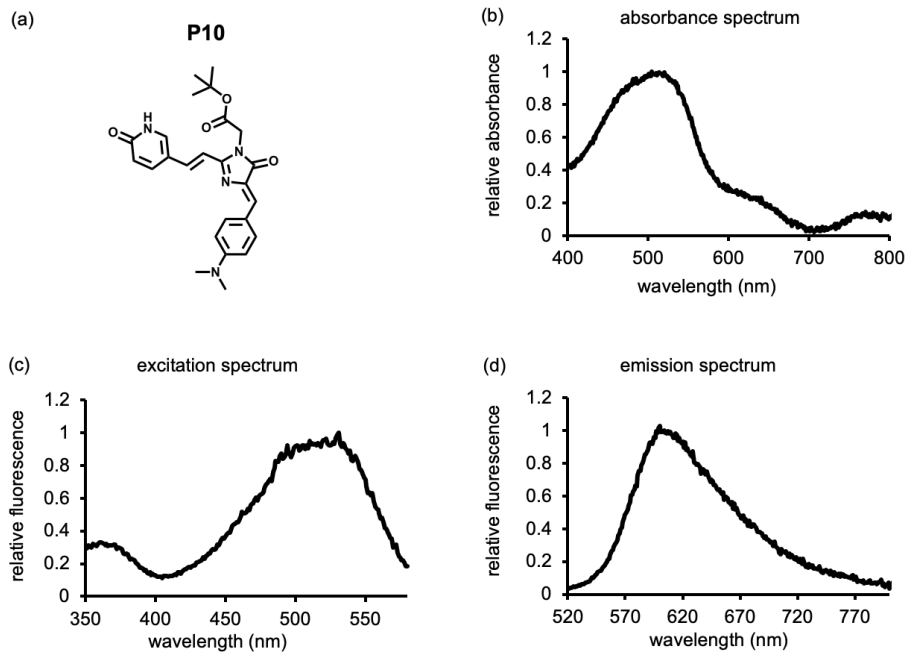

Figure S10: a) Structure of AggFluor P10. **b**) Normalized absorbance spectrum. **c**) Normalized excitation spectrum. **d**) Normalized emission spectrum. All spectra were collected using 10 μM compound in 100% glycerol, 25ºC.

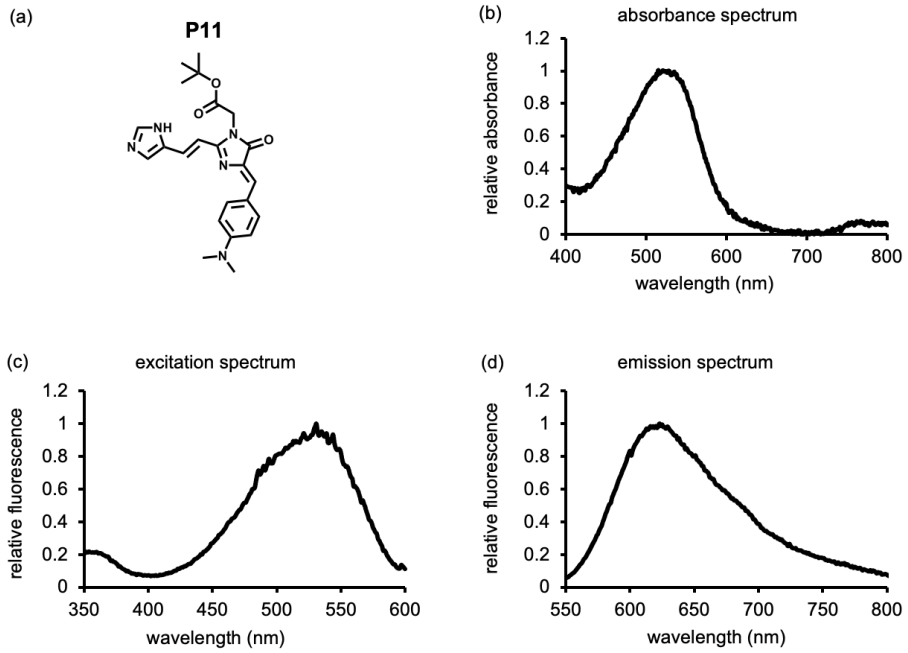

Figure S11: a) Structure of AggFluor P11. **b**) Normalized absorbance spectrum. **c**) Normalized excitation spectrum. **d**) Normalized emission spectrum. All spectra were collected using 10 μM compound in 100% glycerol, 25ºC.

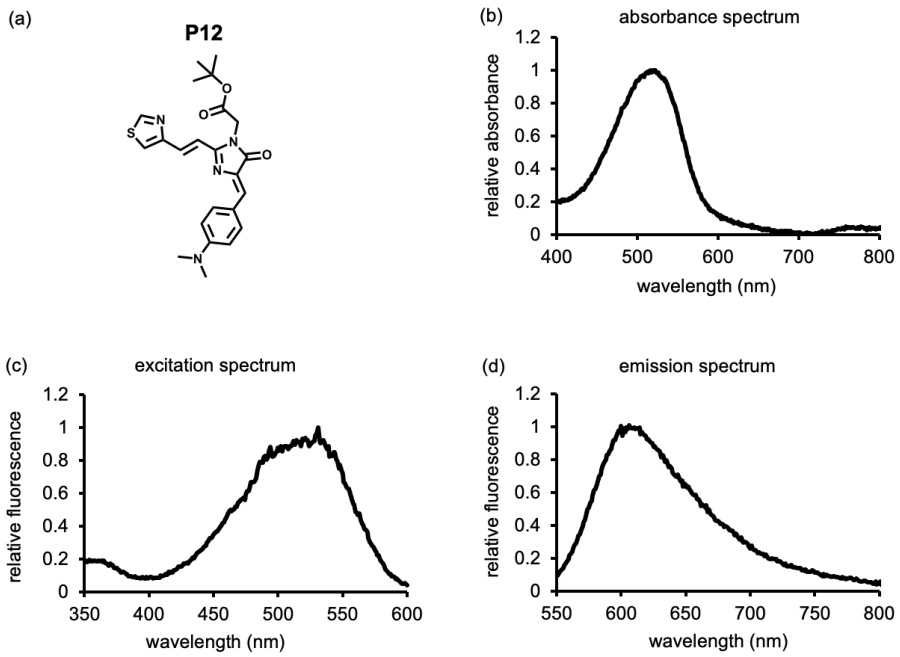

Figure S12: a) Structure of AggFluor P12. **b**) Normalized absorbance spectrum. **c**) Normalized excitation spectrum. **d**) Normalized emission spectrum. All spectra were collected using 10 μM compound in 100% glycerol, 25ºC.

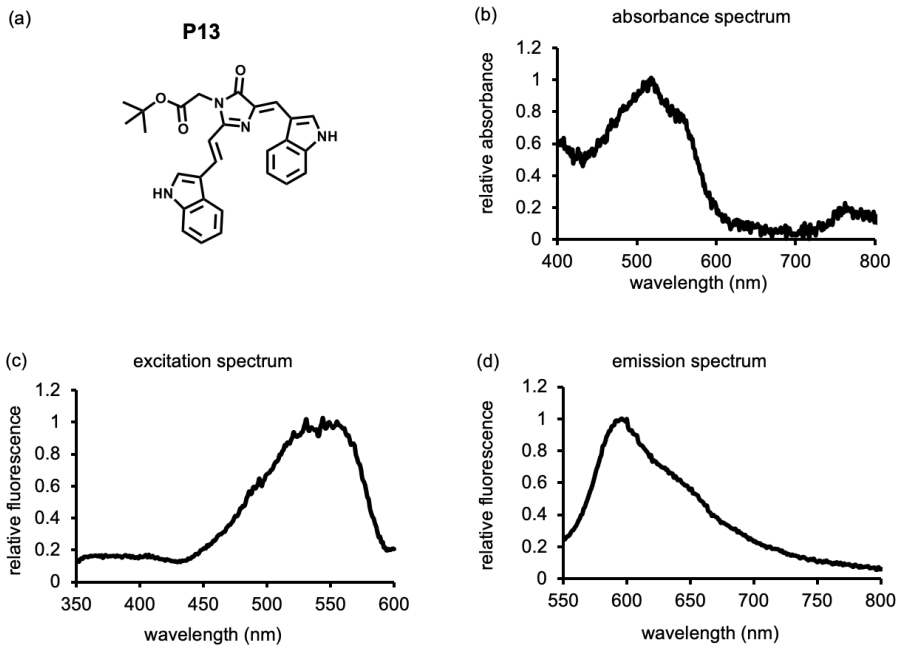

Figure S13: a) Structure of AggFluor P13. **b**) Normalized absorbance spectrum. **c**) Normalized excitation spectrum. **d**) Normalized emission spectrum. All spectra were collected using 10 μM compound in 100% glycerol, 25ºC.

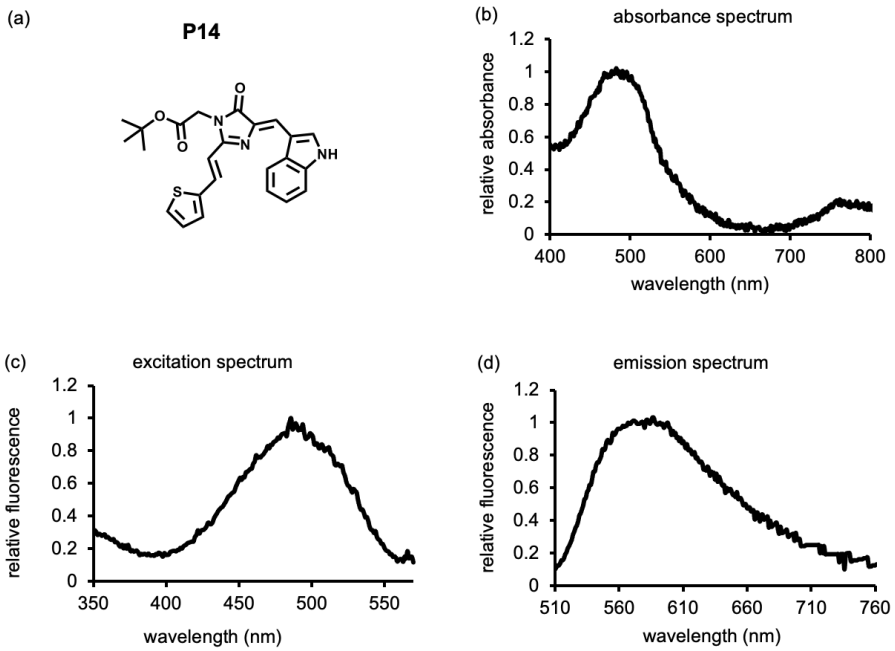

Figure S14: a) Structure of AggFluor P14. **b**) Normalized absorbance spectrum. **c**) Normalized excitation spectrum. **d**) Normalized emission spectrum. All spectra were collected using 10 μM compound in 100% glycerol, 25ºC.

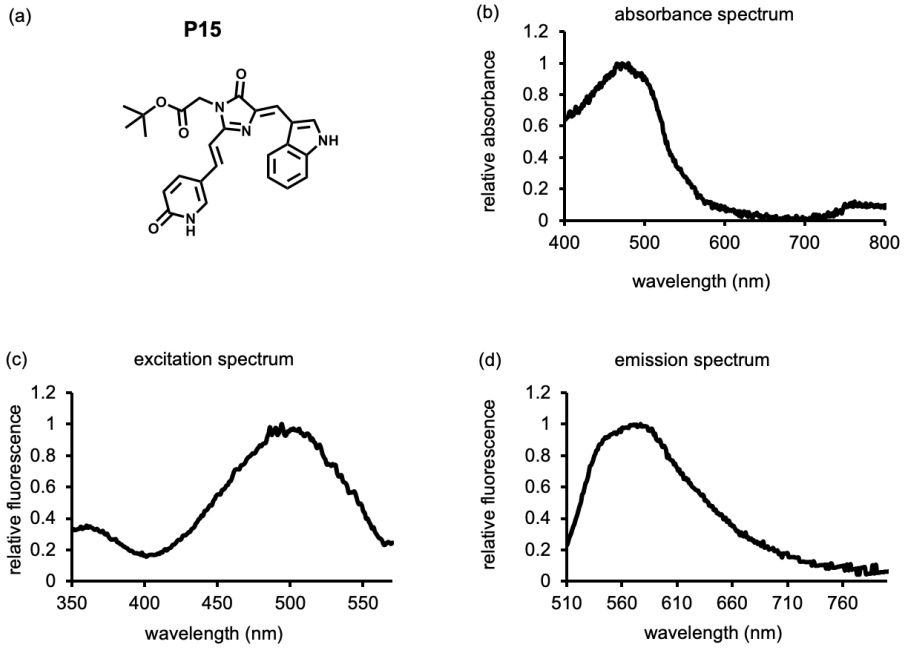

Figure S15: a) Structure of AggFluor P15. **b**) Normalized absorbance spectrum. **c**) Normalized excitation spectrum. **d**) Normalized emission spectrum. All spectra were collected using 10 μM compound in 100% glycerol, 25ºC.

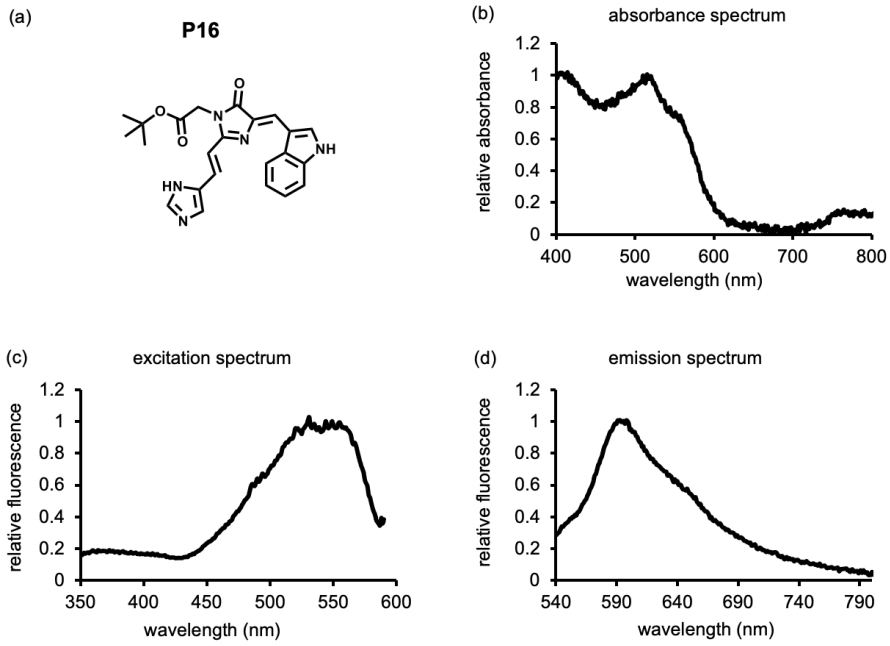

Figure S16: a) Structure of AggFluor P16. **b**) Normalized absorbance spectrum. **c**) Normalized excitation spectrum. **d**) Normalized emission spectrum. All spectra were collected using 10 μM compound in 100% glycerol, 25ºC.

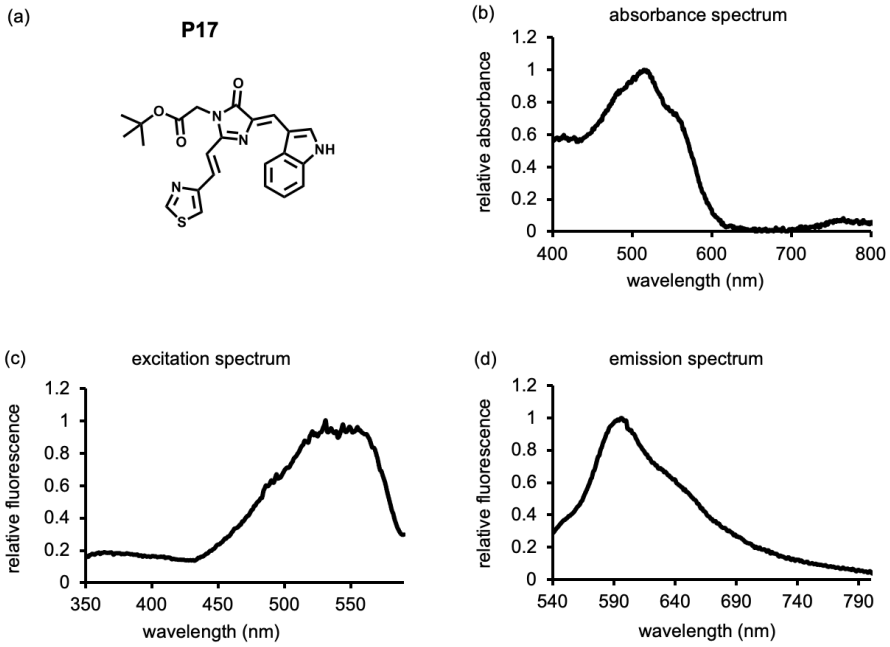

Figure S17: a) Structure of AggFluor P17. **b**) Normalized absorbance spectrum. **c**) Normalized excitation spectrum. **d**) Normalized emission spectrum. All spectra were collected using 10 μM compound in 100% glycerol, 25ºC.

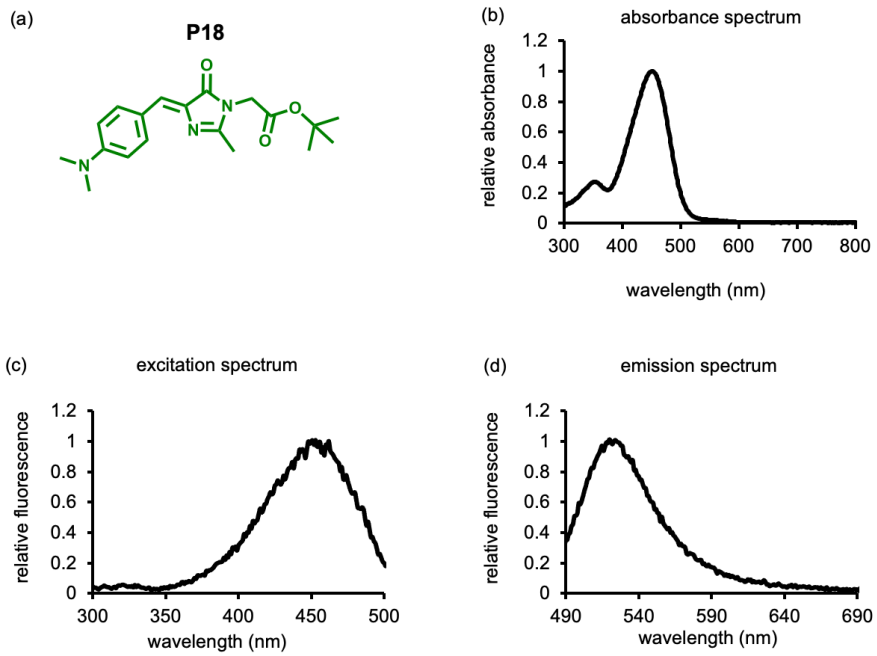

Figure S18: a) Structure of AggFluor P18. **b**) Normalized absorbance spectrum. **c**) Normalized excitation spectrum. **d**) Normalized emission spectrum. All spectra were collected using 10 μM compound in 100% glycerol, 25ºC.

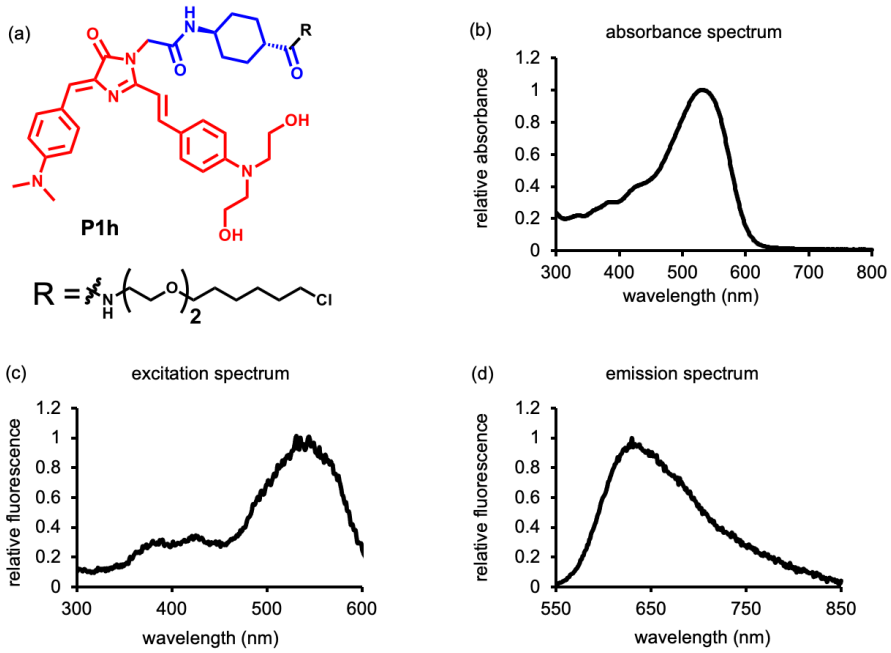

Figure S19: a) Structure of AggFluor P1h. **b**) Normalized absorbance spectrum. **c**) Normalized excitation spectrum. **d**) Normalized emission spectrum. All spectra were collected using 10 μM compound in 100% glycerol, 25ºC.

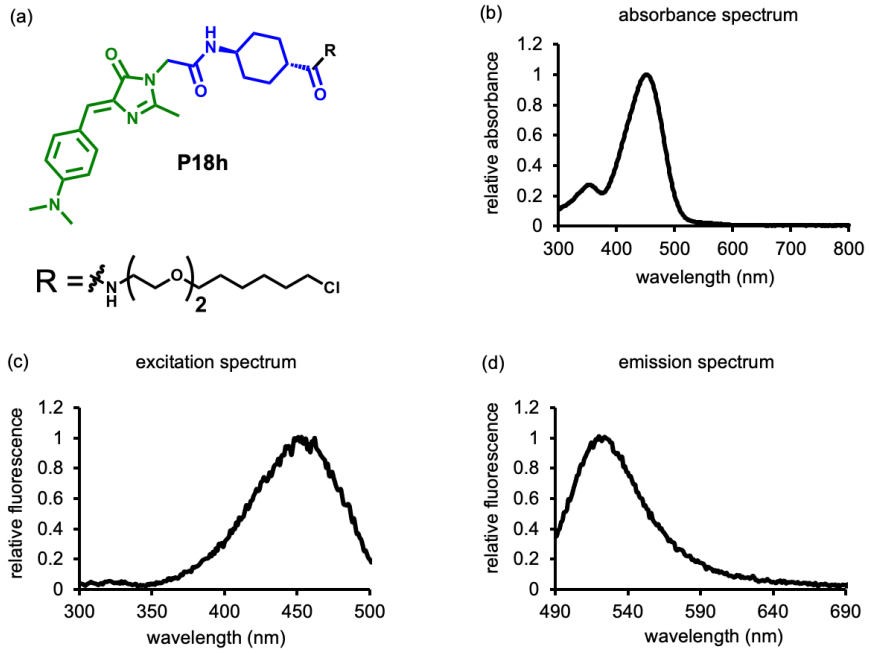

Figure S20: a) Structure of AggFluor P18h. **b**) Normalized absorbance spectrum. **c**) Normalized excitation spectrum. **d**) Normalized emission spectrum. All spectra were collected using 10 μM compound in 100% glycerol, 25ºC.

3.2 Viscosity Sensitivity

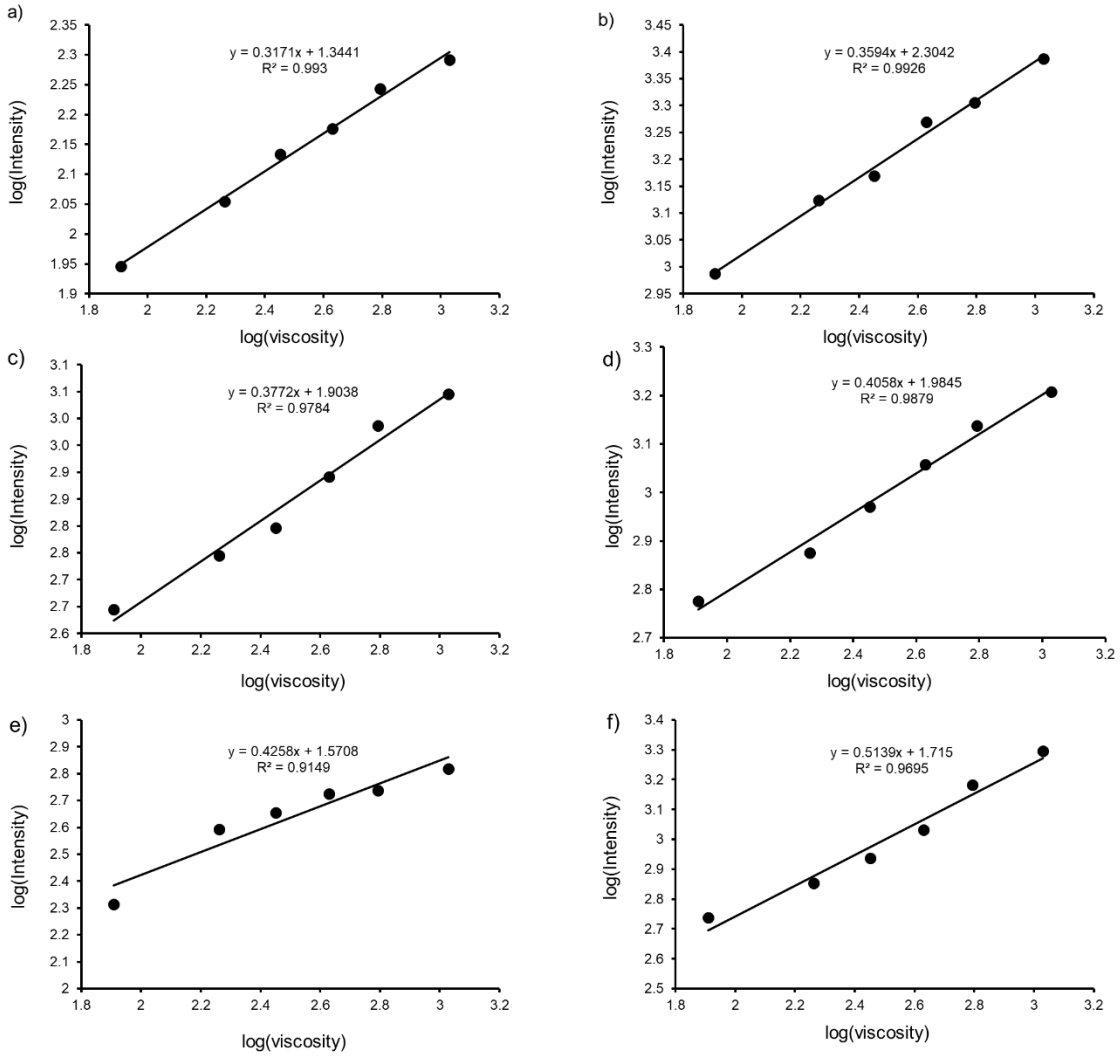

Figure S21: Logarithmic plot of fluorescent intensity as a function of solvent viscosity for P2-7: **a**) P2, **b**) P3, **c**) P4, **d**) P5, **e**) P6, **f**) P7. Fluorescence measurement was carried out using 5 μM compounds in a series of ethylene glycol/glycerol (EG/G) solutions in the following mixing ratios: EG/G = 70/30 (81 cP), 50/50 (183 cP), 40/60 (283 cP), 30/70 (426 cP), 20/80 (621 cP), 0/100 (1069 cp).

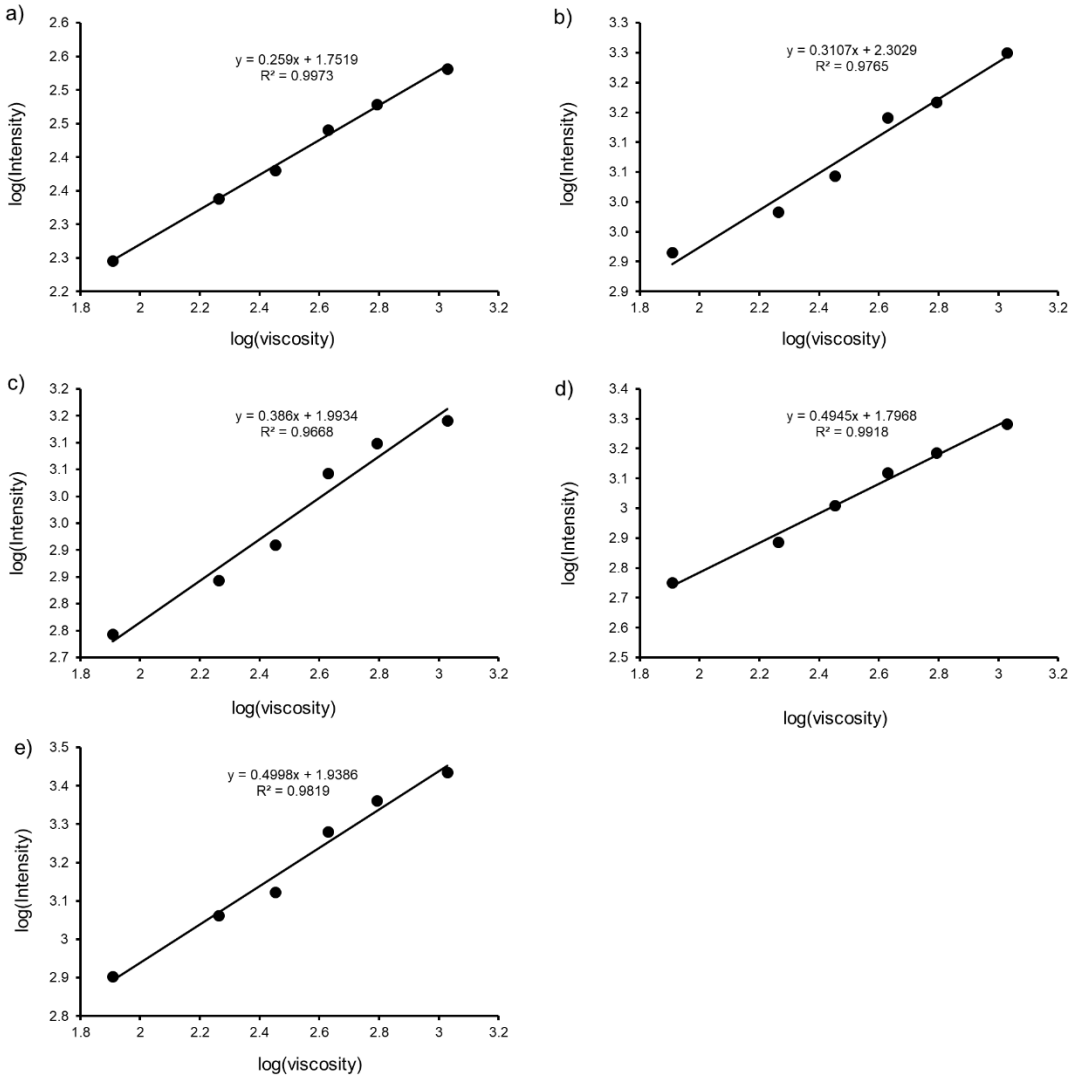

Figure S22: Logarithmic plot of fluorescent intensity as a function of solvent viscosity for P8-P12: **a**) P8, **b**) P9, **c**) P10, **d**) P11, **e**) P12. Fluorescence measurement was carried out using 5 μM compounds in a series of ethylene glycol/glycerol (EG/G) solutions in the following mixing ratios: EG/G = 70/30 (81 cP), 50/50 (183 cP), 40/60 (283 cP), 30/70 (426 cP), 20/80 (621 cP), 0/100 (1069 cp).

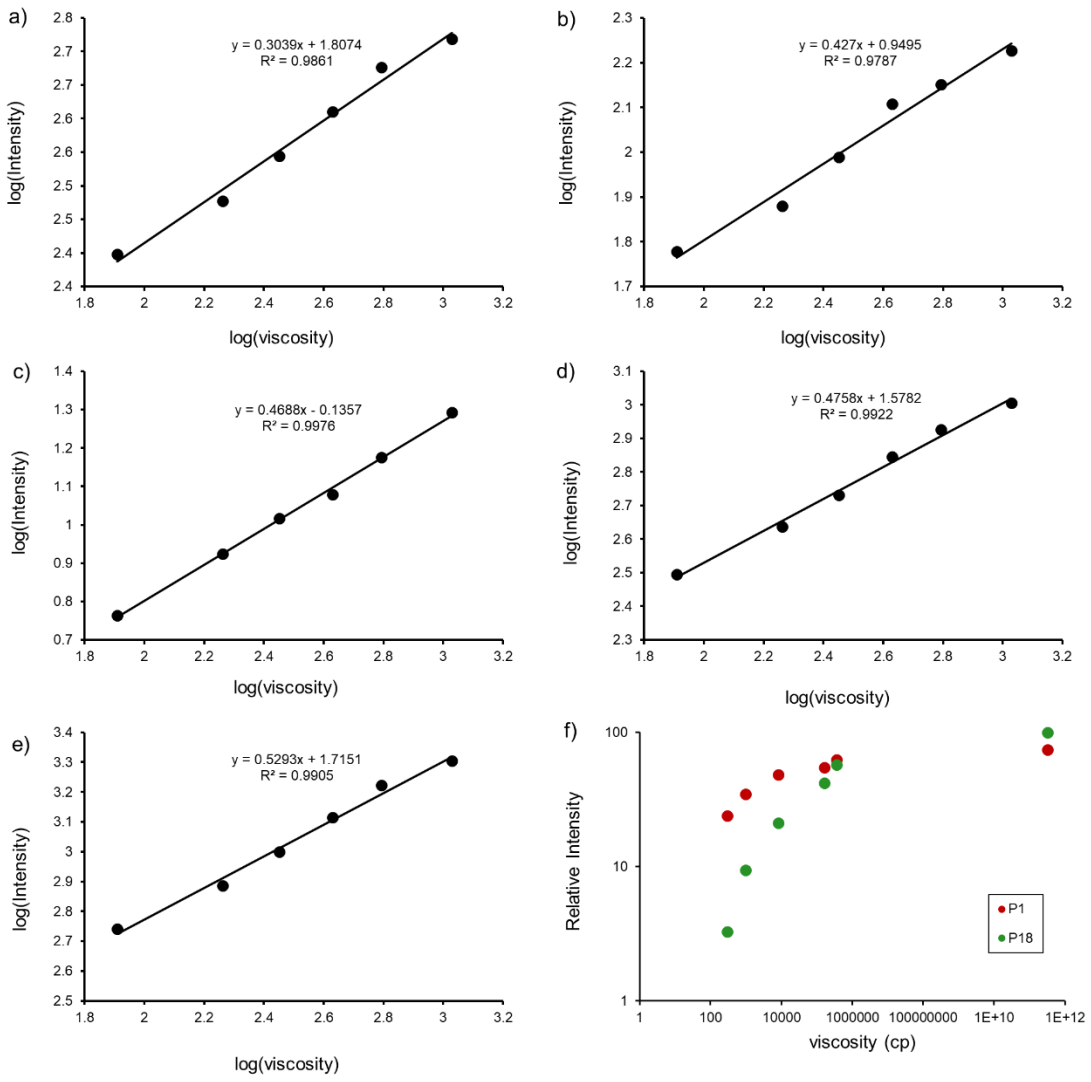

Figure S23: Logarithmic plot of fluorescent intensity as a function of solvent viscosity for P13-17: **a**) P13, **b**) P14, **c**) P15, **d**) P16, **e**) P17. Fluorescence measurement was carried out using 5 μM compounds in a series of ethylene glycol/glycerol (EG/G) solutions in the following mixing ratios: EG/G = 70/30 (81 cP), 50/50 (183 cP), 40/60 (283 cP), 30/70 (426 cP), 20/80 (621 cP), 0/100 (1069 cp). **f**) Logarithmic plot of fluorescent intensity as a function of solvent viscosity for P1 and P18. Fluorescence measurement was carried out using 5 μM compounds in pure glycerol at various temperatures: 37 ˚C, 22 ˚C, 4 ˚C, 0 ˚C, -30 ˚C and -80 ˚C.

3.3 In vitro Protein Aggregation Assays

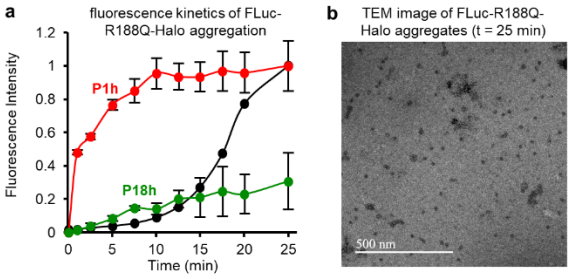

Figure S24: a) Fluorescence and turbidity kinetics of heat-induced Fluc-R188Q-Halo aggregation at 57ºC, 25 µM proteins and 5 µM probes. **b**) TEM images of Fluc-R188Q-Halo aggregates exhibited dispersed and loosely packed structures (57ºC, 25 µM proteins, 20 min).

3.4 Confocal Fluorescence Microscopy

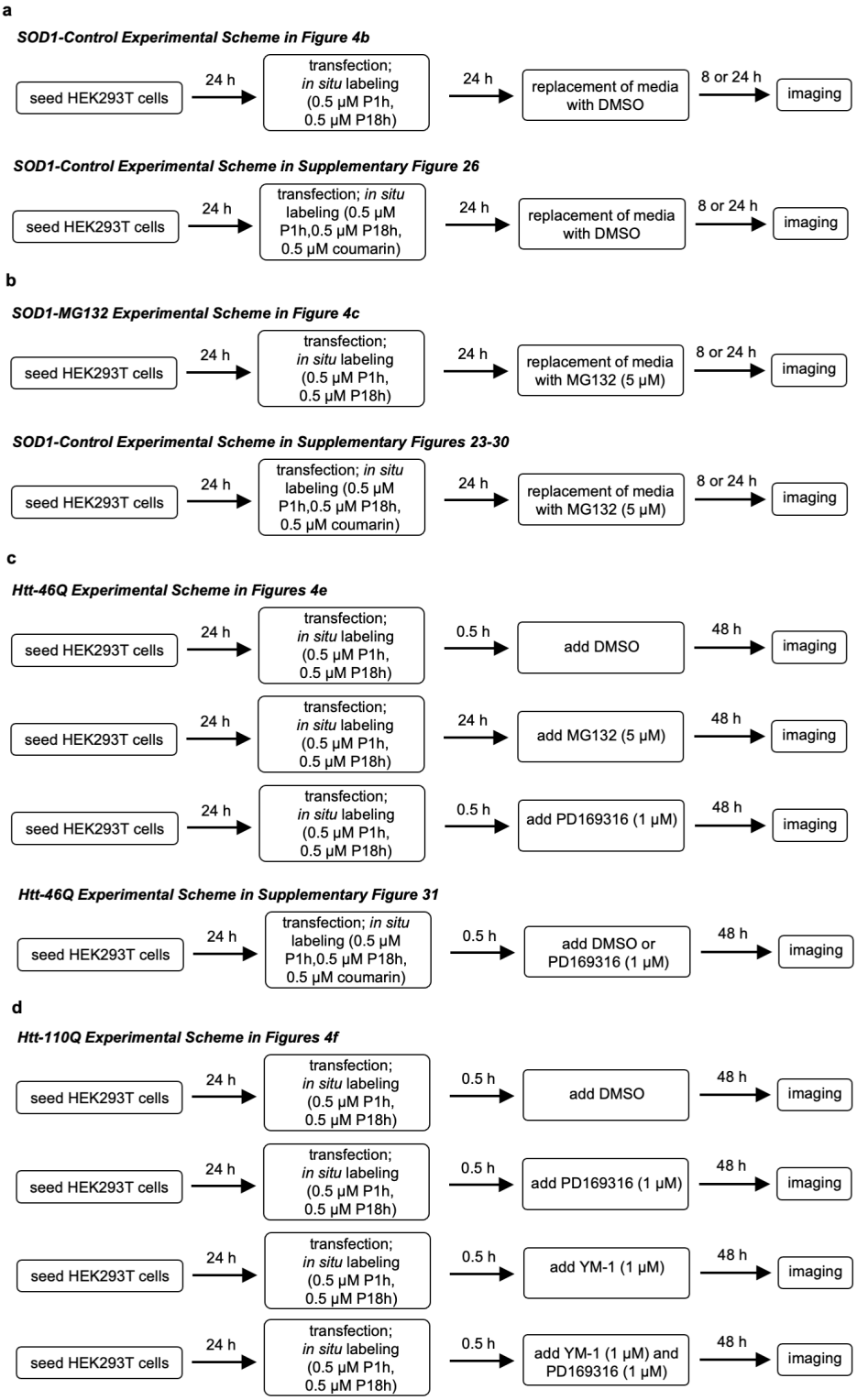

Figure S25: Experimental scheme for confocal fluorescence microscopy experiments.

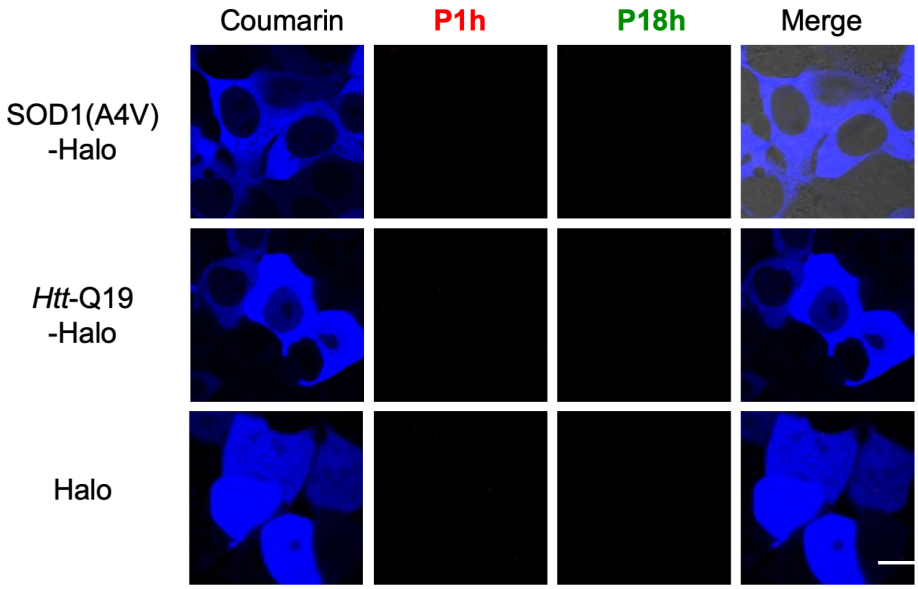

Figure S26: The SOD1(A4V)-Halo, Htt-Q19-Halo and Halo proteins were transiently transfected and expressed in HEK293T cells for 24 h, in the presence of 0.5 μM coumarin Halo-Tag ligand, 0.5 μM P1h and 0.5 μM P18h. Prior to imaging, excess probes were washed away by incubating cells with fresh DMEM media for 30 min at 37 ºC. Only diffuse coumarin fluorescence was observed in cells expressing the POI and no turn-on fluorescence of P1h or P18h was found. Blue: coumarin Halo-Tag ligand. Red: P1h. Green: P18h. Scale bar: 5 μm.

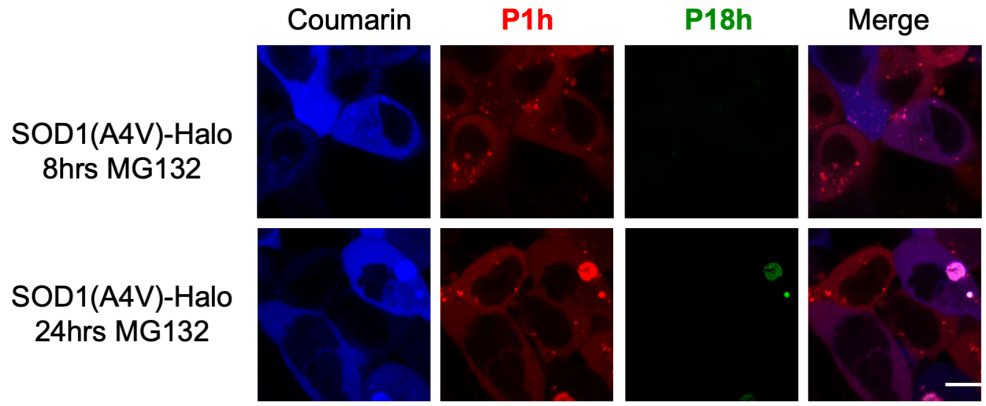

Figure S27: SOD1(A4V)-Halo was transiently transfected and expressed in HEK293T cells for 24 h, in the presence of 0.5 μM coumarin Halo-Tag ligand, 0.5 μM P1h and 0.5 μM P18h. Then, cells were replaced into fresh DMEM media containing 5 μM MG132 to induce proteome aggregation. Cells were treated for 8 or 24 h prior to fluorescence confocal microscopy. Before imaging, excess probes were washed away by incubating cells with fresh DMEM media for 30 min at 37 ºC. Cells stressed with MG132 for 8hrs showed a turn-on fluorescence of P1h, signifying the formation of soluble oligomeric protein aggregates. Whereas, no P18h fluorescence was found at this condition. By contrast, the 24-h stress condition induced turn-on fluorescence of both P1h and P18h, wherein the green fluorescent turn-on of P18h was only found in aggresomes. Blue: coumarin Halo-Tag ligand. Red: P1h. Green: P18h. Scale bar: 5 μm.

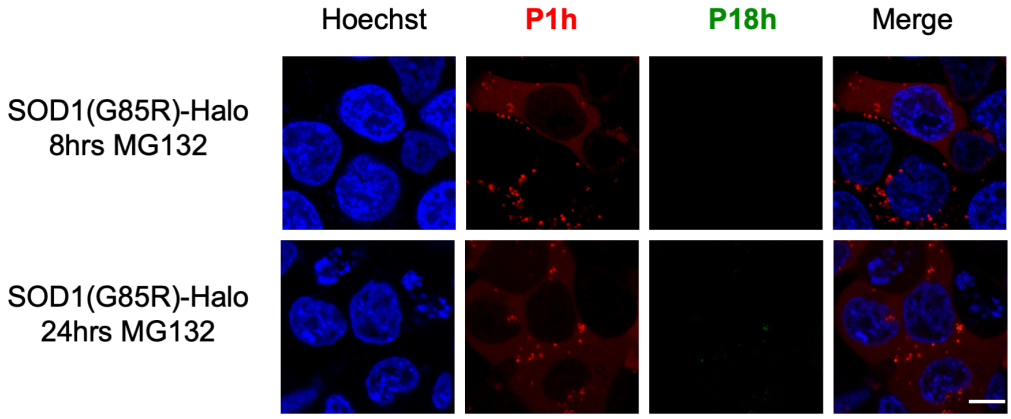

Figure S28: SOD1(G85R)-Halo was transiently transfected and expressed in HEK293T cells for 24 h, in the presence of 0.5 μM P1h and 0.5 μM P18h. Then, cells were replaced into fresh DMEM media containing 5 μM MG132 to induce proteome aggregation. Cells were treated for 8 or 24 h prior to fluorescence confocal microscopy. Before imaging, excess probes were washed away by incubating cells with fresh DMEM supplemented with 0.1 μg/mL Hoechst 33342 for 30 min at 37 ºC. Cells stressed with MG132 for 8hrs showed a turn-on fluorescence of P1h, signifying the formation of soluble oligomeric protein aggregates. Whereas, no P18h fluorescence was found at this condition. The 24-h stress condition induced turn-on fluorescence of P1h. However, the green fluorescent turn-on of P18h was rarely found. Blue: Hoechst 33342. Red: P1h. Green: P18h. Scale bar: 5 μm.

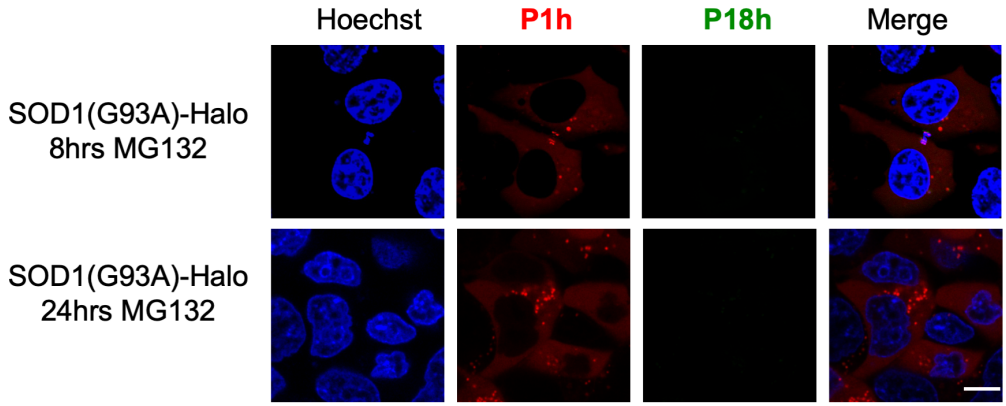

Figure S29: SOD1(G93A)-Halo was transiently transfected and expressed in HEK293T cells for 24 h, in the presence of 0.5 μM P1h and 0.5 μM P18h. Then, cells were replaced into fresh DMEM media containing 5 μM MG132 to induce proteome aggregation. Cells were treated for 8 or 24 h prior to fluorescence confocal microscopy. Before imaging, excess probes were washed away by incubating cells with fresh DMEM supplemented with 0.1 μg/mL Hoechst 33342 for 30 min at 37 ºC. Cells stressed with MG132 for 8hrs showed a turn-on fluorescence of P1h, signifying the formation of soluble oligomeric protein aggregates. Whereas, no P18h fluorescence was found at this condition. The 24-h stress condition induced turn-on fluorescence of P1h. However, no P18h fluorescence was found. Blue: Hoechst 33342. Red: P1h. Green: P18h. Scale bar: 5 μm.

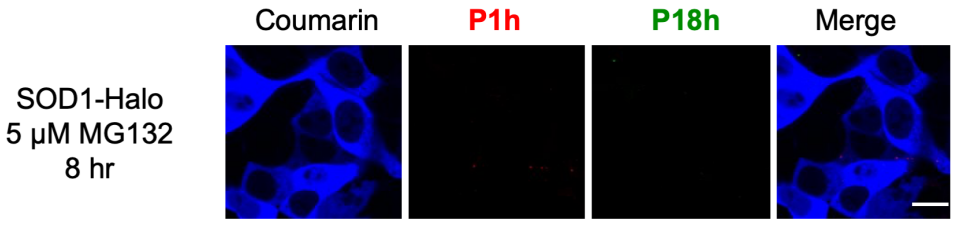

Figure S30: SOD1(WT)-Halo was transiently transfected and expressed in HEK293T cells for 24 h, in the presence of 0.5 μM coumarin Halo-Tag ligand, 0.5 μM P1h and 0.5 μM P18h. Subsequently, excess probes were washed away by incubating cells with fresh DMEM media for 30 min at 37 ºC. Then, cells were replaced into fresh DMEM media containing 5 μM MG132 to induce proteome aggregation. Cells were treated for 8 h prior to fluorescence confocal microscopy. Only diffuse coumarin fluorescence was observed and no turn-on fluorescence of P1h or P18h was found. Blue: coumarin Halo-Tag ligand. Red: fluorescence of P1h. Green: fluorescence of P18h. Scale bar: 5 μm.

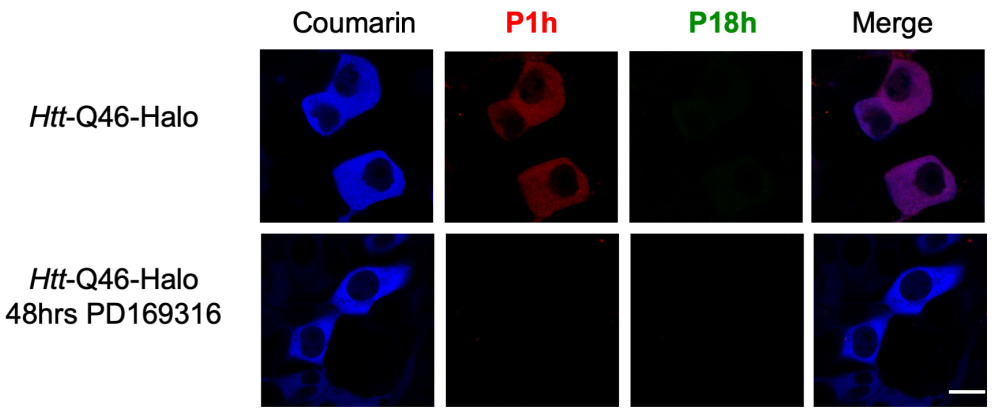

Figure S31: Htt-Q46-Halo was transiently transfected and expressed in HEK293T cells for 48 h, with or without 1 μM PD169316, in the presence of 0.5 μM coumarin Halo-Tag ligand, 0.5 μM P1h and 0.5 μM P18h. Subsequently, excess probes were washed away by incubating cells with fresh DMEM media for 30 min at 37 ºC. Cells expressing Htt-Q46-Halo, which is known to form predominantly soluble oligomeric protein species, show diffuse coumarin fluorescence along with an obvious turn-on of red fluorescence of P1h, with not fluorescence from P18h. In the presence of PD169316, cells show only diffusive coumarin fluorescence, indicating presence of proteins. However, there was no fluorescence observed in the channels of P1h and P18h, indicating the clearance of protein aggregates. Blue: coumarin Halo-Tag ligand. Red: fluorescence of P1h. Green: fluorescence of P18h. Scale bar: 5 μm.

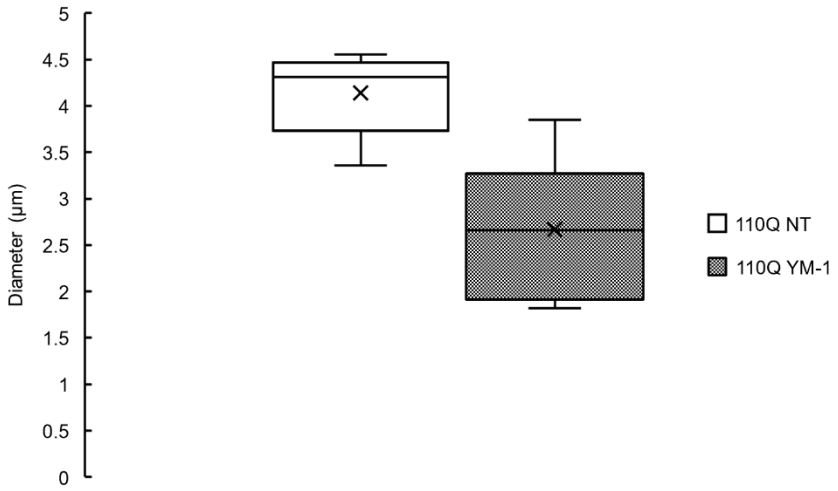

Figure S32: Htt-Q110-Halo was transiently transfected and expressed in HEK293T cells for 48 h with or without 1 µM of Hsp70 activator YM-1, in the presence of 0.5 µM of P1h and 0.5 µM of P18h. Subsequently, excess probes were washed away by incubating cells with fresh DMEM media for 30 min at 37 ºC. Using Zen Blue profile application, the pixel length of the 110Q puncta was determined using green fluorescence from P18h, which was then converted to the unit of nm using ratio of 0.07µm/pixel. The average diameter of non-treated 110Q puncta was determined to be 4.1 ± 0.45 µm and YM-1 treated 110Q puncta showed average diameter of 2.6 ± 0.75 µm. (n = 6 for each)

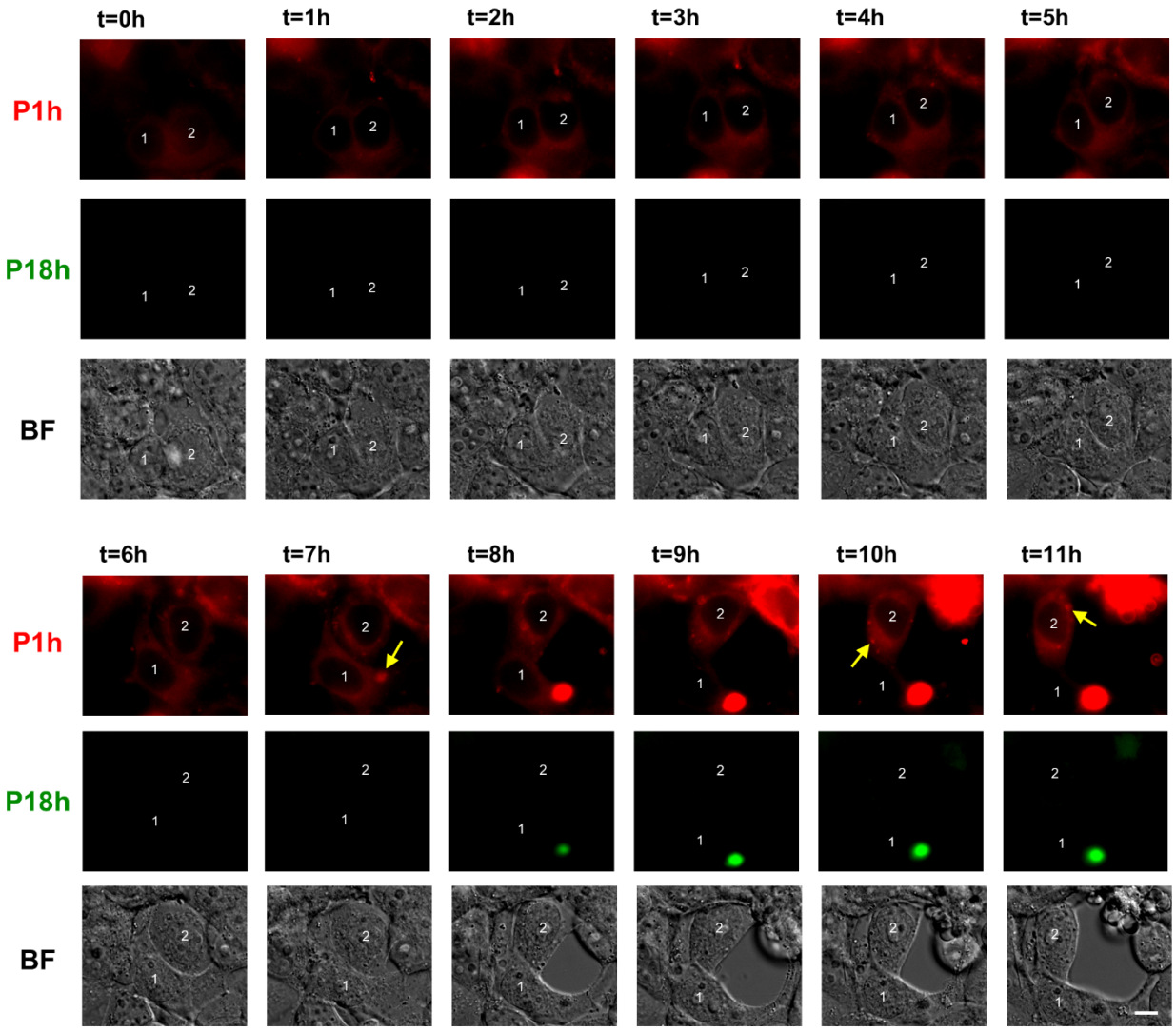

Figure S33: Htt-Q72-Halo was transiently transfected and expressed in HEK293T cells for 36 h in the presence of 0.5 μM P1h and 0.5 μM P18h. Then, cells were replaced into fresh DMEM media containing 5 μM MG132 to induce proteome aggregation and imaged over the course of 12 h. The time-lapse imaging experiment revealed that misfolding oligomers appear first, with diffuse P1h signal observed the beginning of imaging. At the 7-h time point, the P1h signal shows that misfolded oligomers begin to condense to form aggresome-like structures near the nucleus. Signal from P18h started to appear around the 8-h time point and the signal originated from the core of the aggresome. In addition to aggresomes, small puncta structures with no P18h green fluorescence were also found at final time points at 10 or 11 h, suggesting that these granules containing misfolded oligomers were in the process to form insoluble aggregates. Red: fluorescence of P1h. Green: fluorescence of P18h. Scale bar: 5 μm.

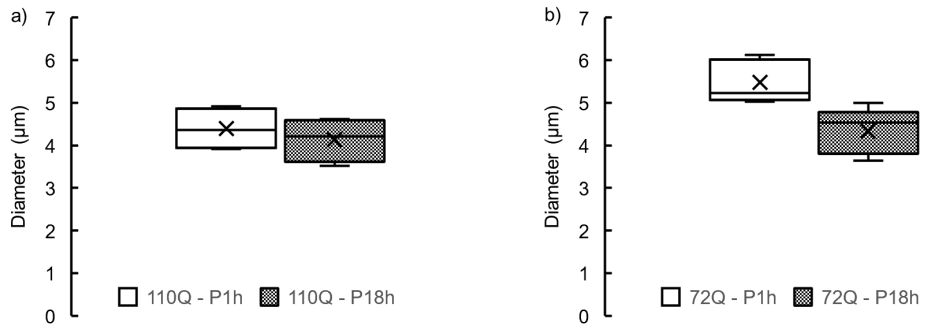

Figure S34: a) Htt-Q110-Halo was transiently transfected and expressed in HEK293T cells for 48 h in the presence of 0.5 μM of P1h and 0.5 μM of P18h. Then, cells were replaced into fresh DMEM and imaged. Cells expressing Htt-Q110-Halo formed perinuclear granular aggresomes that are detected by P1h and P18h. The average diameter 110Q puncta determined via P1h fluorescence to be 4.4 ± 0.43 μm and by P18h fluorescence had an average diameter of 4.1 ± 0.45 μm (n = 6 for each). **b)** Htt-Q72-Halo was transiently transfected and expressed in HEK293T cells for 36 h in the presence of 0.5 μM of P1h and 0.5 μM of P18h. Then, cells were replaced into fresh DMEM media containing 5 μM MG132 to induce proteome aggregation and imaged after 12 h. Cells expressing Htt-Q72-Halo, which is known to forms mainly soluble oligomeric protein species, which can be driven to form perinuclear granular aggresomes that are detected by P1h and P18h. Using Zen Blue profile analyses, the average diameter of MG132 induced 72Q puncta determined via P1h fluorescence to be 5.5 ± 0.50 μm and by p18h fluorescence had an average diameter of 4.3 ± 0.54 μm (n = 6 for each).

4. Synthetic Methods and Schemes

4.1 General Methods.

All reagents and anhydrous solvents of commercial grade were used as received unless otherwise states. Reaction progress was monitored by thin layer chromatography (TLC) analysis using Silicycle® glass backed, extra hard sheets (60 Å, 250 μm thickness). Reaction components were detected by UV-absorption (254 or 365 nm) or by the indicated stain. Purifications by way of flash column chromatography were completed using SiliaFlash® F60 (40-63 μm) eluting with the indicated solvent mixture. ^{1}H-NMR and ^{13}C-NMR characterization of isolated products was completed using a Bruker AV-III-HD-500 spectrometer in chloroform-*d* ($CDCl_3$) or d_6-dimethylsulfoxide (DMSO-d_6) unless otherwise noted. Chemical shifts (δ) are reported relative to a tetramethylsilane (TMS) standard (δ 0.00 ppm) or to that of the solvent residual peak. Coupling constants (*J*) are reported in Hz. All ^{13}C-NMR spectra are reported as proton decoupled. High resolution mass spectrometry was completed with a Waters Q-TOF Premier quadrupole/time-of-flight (TOF) mass spectrometer. M

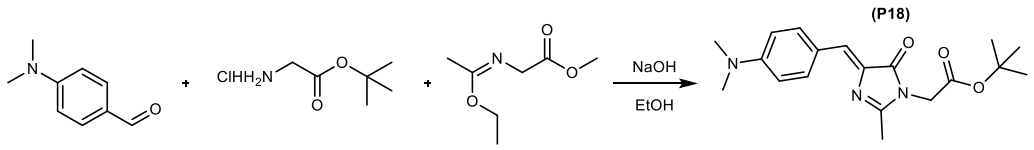

Scheme S1: Synthesis of P18

Conditions: glycine *tert*-butyl ester hydrochloride (183.7 mg, 1.1 mmol) was combine with NaOH (39.9 mg, 1 mmo1) in EtOH (2 mL) and stirred for 1 hr. at room temperature. 4-(Dimethylamino)benzaldehyde (149.0 mg, 1.0 mmol) was added and stirred overnight and 25˚C. Methyl (Z)-2-((1-ethoxyethylidene)amino)acetate (159mg, 1.0 mmol) was prepared according to literature and added in one portion[11]. The reaction was stirred overnight at 25˚C, was then quenched by water (5 mL) and extracted with ether (3x10 mL). The organic fraction was collected and dried in vacuo. Compounds were further purified by flash chromatography (50% Ethyl Acetate, 50% Hexanes) to yield P18 an orange solid.

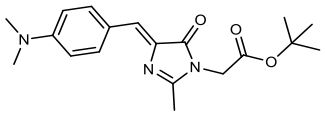

P18: (Z)-tert-butyl 2-(4-(4-(dimethylamino)benzylidene)-2-methyl-5-oxo-4,5-dihydro-1H-imidazol-1-yl)acetate. Crystalline orange solid (63%).

^{1}H NMR (500 MHz, Chloroform-*d*) δ 8.07 (d, *J* = 8.9 Hz, 2H), 7.11 (s, 1H), 6.70 (d, *J* = 8.8 Hz, 2H), 4.29 (s, 2H), 3.05 (s, 6H), 2.31 (s, 3H), 1.48 (s, 9H). ^{13}C NMR (126 MHz, Chloroform-d) δ 170.12, 166.91, 158.04, 151.58, 134.28, 134.24, 129.42, 122.20, 111.73, 82.84, 42.15, 40.05, 27.99, 15.43. [M+H] Calcd, 344.1896; Obsd, 344.1983

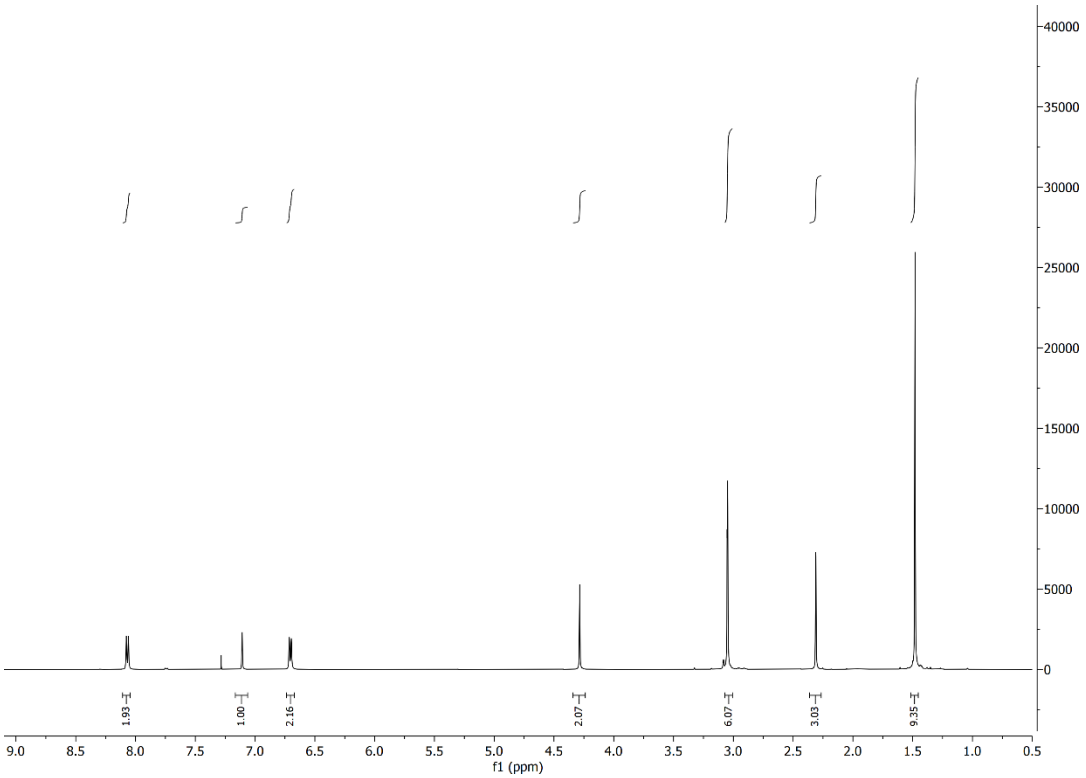
1.93
1.00
2.16
2.07
6.07
3.03
9.35
f1 (ppm)

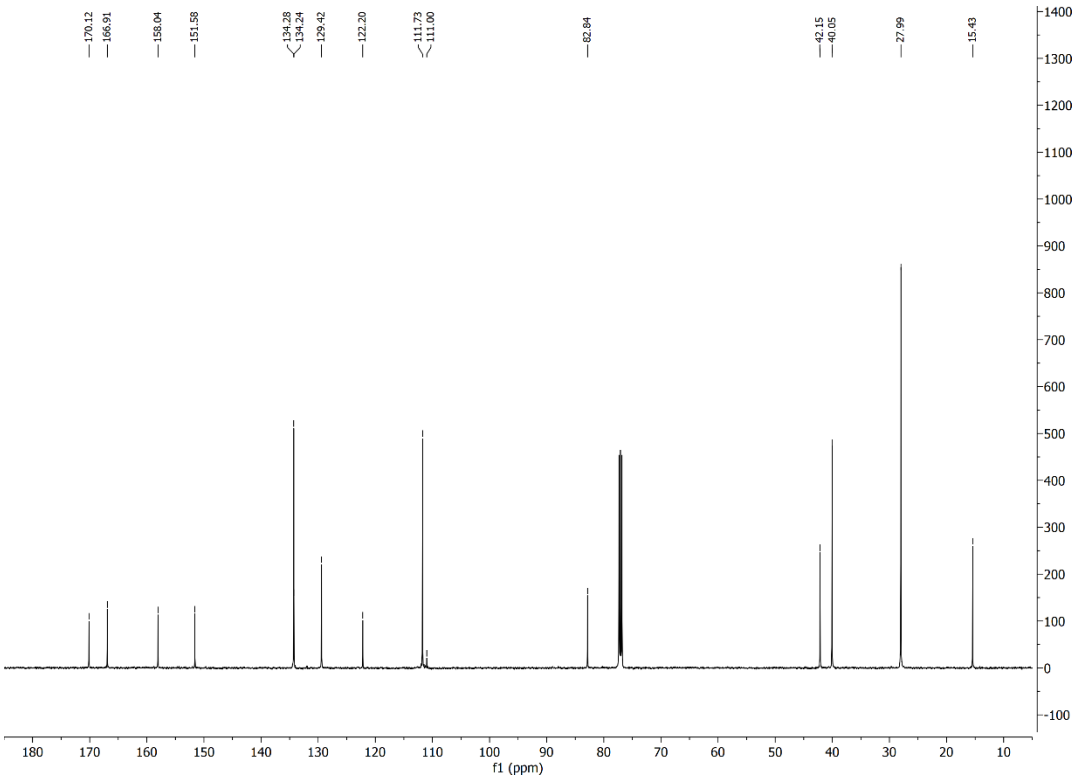
170.12
166.91
158.04
151.58
134.28
134.24
129.42
122.20
111.73
111.00
82.84
42.15
40.05
27.99
15.43
f1 (ppm)

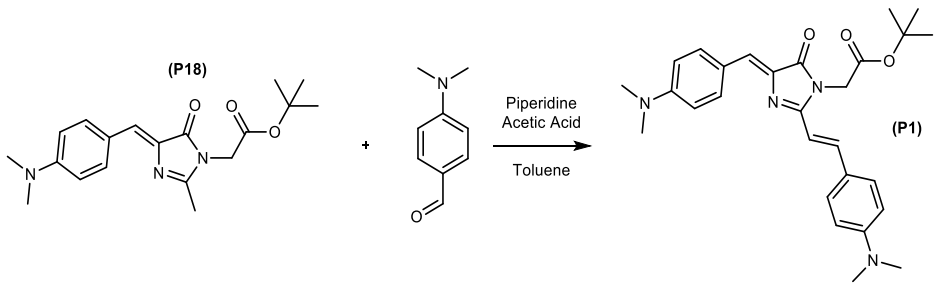

Scheme S2: Synthesis of P1

Conditions: 4-(Dimethylamino)benzaldehyde (223.3 mg, 1.5 mmol), P18 (343.0 mg, 1.0 mmol) were combine in toluene (2 mL) under Argon. Piperidine (824 µL, 8.0 mmol) and then acetic acid (458 µL, 8.0 mmol) were added and the reaction was refluxed at 110˚C overnight. Solvent was removed and was purified by flash chromatography (50% Ethyl Acetate, 50% Hexanes) to yield P1 a red solid.

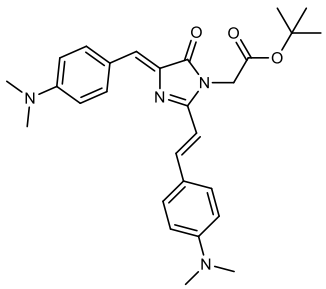

P1: Tert-butyl 2-((Z)-4-(4-(dimethylamino)benzylidene)-2-((E)-4-(dimethylamino)styryl)-5-oxo-4,5-dihydro-1H-imidazol-1-yl)acetate. Red Solid (44%).

^{1}H NMR (500 MHz, Chloroform- *d*) δ 8.19 (d, J = 8.6 Hz, 2H), 7.97 (d, J = 15.6 Hz, 1H), 7.48 (d, J = 8.7, 2H), 7.12 (s, 1H), 6.75 (d, J = 8.6 , 2H), 6.70 (d, J = 8.6, 2H), 6.42 (d, J = 15.6 Hz, 1H), 4.45 (s, 2H), 3.07 (s, 6H), 3.05 (s, 6H), 1.49 (m, 9H). ^{13}C NMR (126 MHz, Chloroform-*d*) δ 170.38, 167.13, 156.62, 151.44, 151.35, 139.94, 135.55, 134.32, 129.42, 127.64, 123.54, 123.22, 111.96, 111.86, 111.72, 107.59, 82.73, 42.38, 40.17, 40.11, 40.03, 28.03, 28.01, 27.98. [M+H] Calcd, 475.2664; Obsd, 475.3517

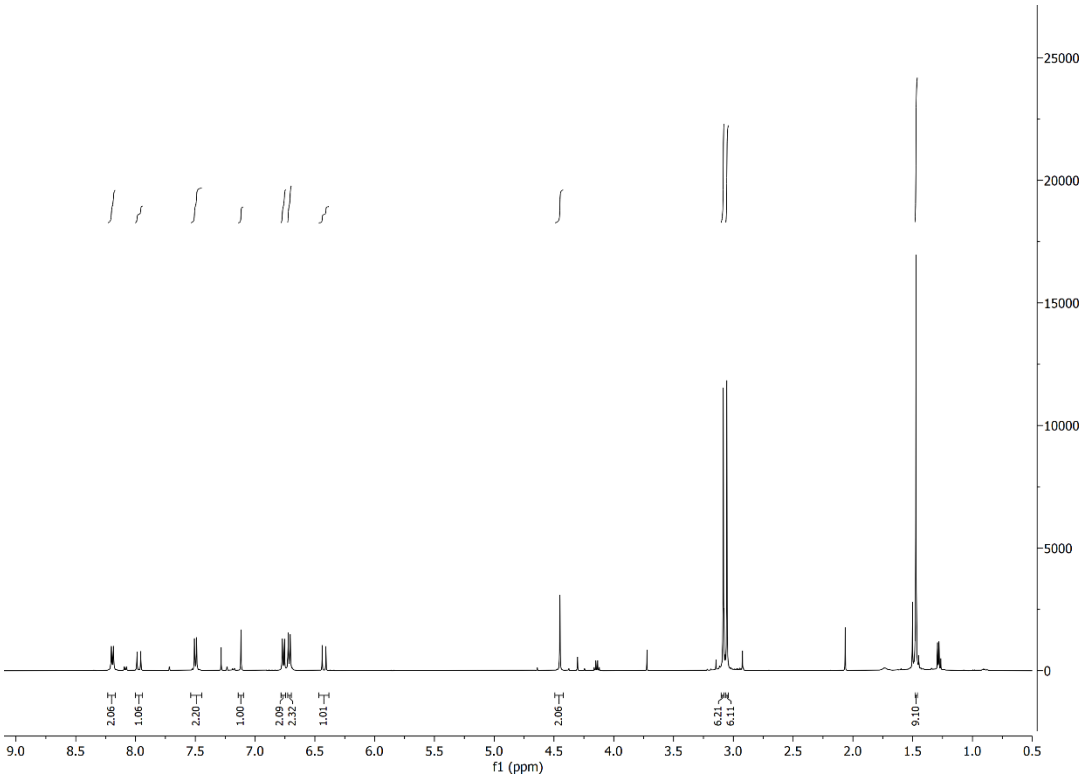
2.06
1.06
2.20
1.00
2.09
2.32
1.01
2.06
6.21
6.11
9.10
f1 (ppm)

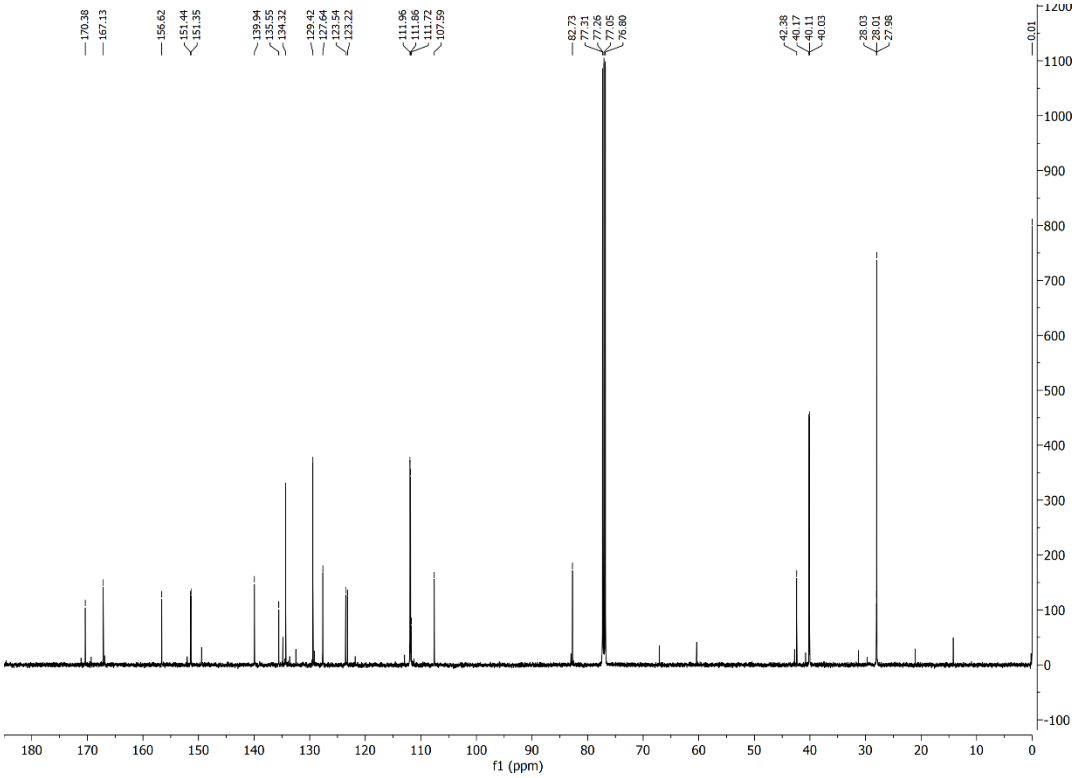
170.38
167.13
156.62
151.44
151.35
139.94
135.55
134.32
129.42
127.64
123.54
123.22
111.96
111.86
111.72
107.59
82.73
77.31
77.26
77.05
76.80
42.38
40.17
40.11
40.03
28.03
28.01
27.98
0.01
f1 (ppm)

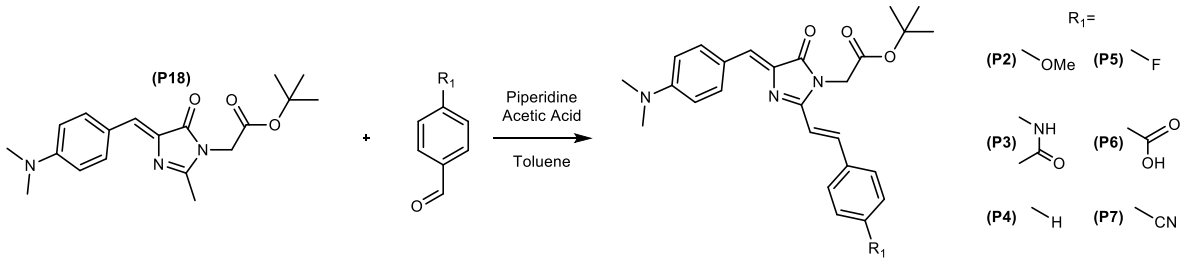

Scheme S3: Synthesis of P2-P7

Conditions: benzaldehyde (1.5 mmol), P18 (343.0 mg, 1 mmol) were combine in toluene (2 mL) under Argon. Piperidine (824 µL, 8.0 mmol) and then acetic acid (458 µL, 8.0 mmol) were added and the reaction was refluxed at 110˚C overnight. Solvent was removed and was purified by flash chromatography (various conditions) to yield P2-P7**.**

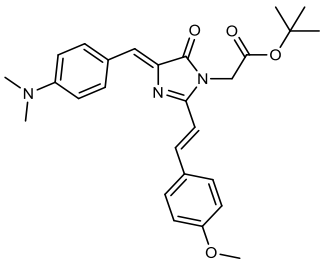

P2: Tert-butyl 2-(4-((Z)-4-(dimethylamino)benzylidene)-2-((E)-4-methoxystyryl)-5-oxo-4,5-dihydro-1H-imidazol-1-yl)acetate. Red Solid (37%).

^{1}H NMR (500 MHz, $CDCl_3$) δ 8.20 (d, *J* = 8.6 Hz, 2H), 7.98 (d, *J* = 15.7 Hz, 1H), 7.55 (d, 2H), 7.17 (s, 1H), 6.95 (d, 2H), 6.77 (d, *J* = 8.9 Hz, 2H), 6.53 (d, *J* = 15.7 Hz, 1H), 4.46 (s, 2H), 3.88 (s, 3H), 3.10 (s, 6H), 1.48 (s, 9H). ^{13}C NMR (126 MHz, $CDCl_3$) δ 134.56, 129.31, 114.43, 111.84, 55.42, 40.12, 31.95, 29.72, 27.98, 22.71, 14.15, 1.04. [M+H] Calcd, 462.2388; Obsd, 462.2385

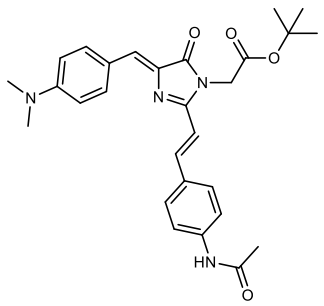

P3: tert-butyl 2-(2-((E)-4-acetamidostyryl)-4-((Z)-4-(dimethylamino)benzylidene)-5-oxo-4,5-dihydro-1H-imidazol-1-yl)acetate. Red Solid (31%).

^{1}H NMR (500 MHz, $CDCl_3$) δ 8.33 (s, 1H), 8.10 (d, *J* = 6.6 Hz, 2H), 8.03 (d, *J* = 15.9, 2.5 Hz, 1H), 7.58 (d, *J* = 7.7 Hz, 2H), 7.51 (d, *J* = 7.9 Hz, 2H), 7.19 (s, 1H), 6.76 (d, *J* = 8.6, 3.4 Hz, 2H), 6.58 (d, *J* = 15.8, 4.4 Hz, 1H), 4.51 (s, 2H), 3.10 (s, 6H), 2.21 (s, 3H), 1.49 (s, 9H). ^{13}C NMR (126 MHz, $CDCl_3$) δ 166.66, 155.62, 152.03, 134.96, 130.11, 129.89, 129.12, 122.06, 119.86, 112.08, 111.76, 84.35, 83.45, 42.36, 40.22, 40.19, 29.72, 27.98, 24.66, 22.71, 14.15. [M+H] Calcd, 489.2497; Obsd, 489.2496

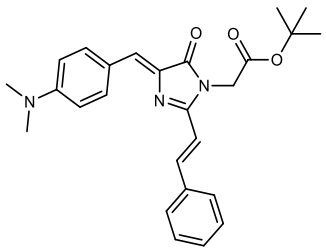

P4: Tert-butyl 2-(4-((Z)-4-(dimethylamino)benzylidene)-5-oxo-2-((E)-styryl)-4,5-dihydro-1H-imidazol-1-yl)acetate. Red solid (15%).

^{1}H NMR (500 MHz, $CDCl_3$) δ 8.20 (d, *J* = 8.5 Hz, 2H), 8.01 (d, *J* = 15.9 Hz, 1H), 7.60 (d, 2H), 7.46 – 7.37 (m, 5H), 7.20 (s, 1H), 6.68 (d, *J* = 15.8 Hz, 1H), 4.47 (s, 2H), 3.73 (s, 6H), 1.48 (s, 9H). ^{13}C NMR (126 MHz, $CDCl_3$) δ 171.20, 170.13, 167.01, 155.57, 151.69, 139.14, 135.55, 135.02, 134.72, 129.74, 128.96, 127.68, 122.81, 113.31, 111.84, 82.94, 67.10, 60.43, 53.45, 42.33, 40.11, 31.95, 30.96, 29.72, 29.38, 27.98, 22.72, 21.08, 14.22, 14.15, 1.94, 1.04. [M+H] Calcd, 432.2282; Obsd, 432.2281

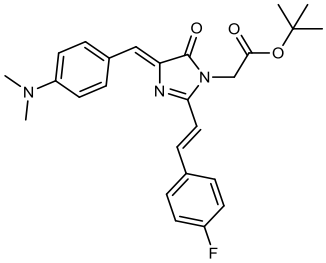

P5: Tert-butyl 2-(4-((Z)-4-(dimethylamino)benzylidene)-2-((E)-4-fluorostyryl)-5-oxo-4,5-dihydro-1H-imidazol-1-yl)acetate. Red solid (21%).

^{1}H NMR (500 MHz, $CDCl_3$) δ 8.20 (d, *J* = 8.5 Hz, 2H), 8.01 (d, *J* = 15.9 Hz, 1H), 7.60 (d, 2H), 7.46 – 7.37 (m, 5H), 7.20 (s, 1H), 6.68 (d, *J* = 15.8 Hz, 1H), 4.47 (s, 2H), 3.73 (s, 6H), 1.48 (s, 9H). ^{13}C NMR (126 MHz, $CDCl_3$) δ 168.92, 166.66, 165.29, 164.84, 162.84, 155.52, 151.84, 149.90, 146.23, 140.60, 139.65, 137.15, 134.96, 132.42, 131.54, 131.51, 131.04, 130.96, 130.27, 129.83, 129.76, 122.61, 116.68, 116.50, 116.43, 116.30, 116.12, 112.23, 111.89, 111.87, 111.81, 83.24, 42.37, 42.32, 40.31, 40.23, 29.71, 29.10, 27.96, 26.27, 22.71, 14.14, 1.93. [M+H] Calcd, 450.2188; Obsd, 450.2188

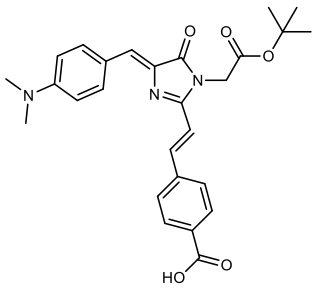

P6: 4-((E)-2-(1-(2-(tert-butoxy)-2-oxoethyl)-4-((Z)-4-(dimethylamino)benzylidene)-5-oxo-4,5-dihydro-1H-imidazol-2-yl)vinyl)benzoic acid. Red solid (40%).

^{1}H NMR (500 MHz, MeOD) δ 8.21 (d, *J* = 8.7 Hz, 2H), 8.09 (d, 2H), 8.02 (d, *J* = 15.8 Hz, 1H), 7.82 (d, 2H), 7.15 (s, 1H), 7.12 (d, *J* = 15.9 Hz, 1H), 6.85 (d, 2H), 4.62 (s, 2H), 3.14 (s, 6H), 1.49 (s, 9H). 13C NMR (126 MHz, MeOD) δ 167.40, 134.90, 129.95, 127.43, 122.20, 111.52, 82.54, 66.74, 38.77, 31.69, 29.36, 29.09, 26.81, 22.35, 13.05, 1.44. [M+H] Calcd, 476.2180; Obsd, 476.2140

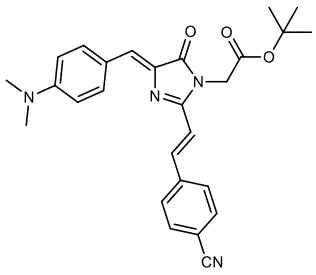

P7: Tert-butyl 2-(2-((E)-4-cyanostyryl)-4-((Z)-4-(dimethylamino)benzylidene)-5-oxo-4,5-dihydro-1H-imidazol-1-yl)acetate. Red solid (33%).

^{1}H NMR (500 MHz, $CDCl_3$) δ 8.20 (d, *J* = 8.6 Hz, 2H), 7.97 (d, *J* = 15.7 Hz, 1H), 7.71 (d, 2H), 7.67 (d, *J* = 8.4 Hz, 2H), 7.25 (s, 1H), 6.79 – 6.74 (m, 3H), 4.48 (s, 2H), 3.12 (s, 6H), 1.48 (s, 9H).

^{13}C NMR (126 MHz, $CDCl_3$) δ 169.81, 166.97, 154.51, 151.95, 139.85, 136.30, 135.04, 134.70, 132.71, 131.11, 127.91, 122.61, 118.58, 116.84, 112.56, 111.86, 83.12, 42.26, 40.11, 31.95, 29.72, 29.39, 27.99, 22.72, 14.15, 1.04. [M+H] Calcd, 457.2234; Obsd, 457.2234

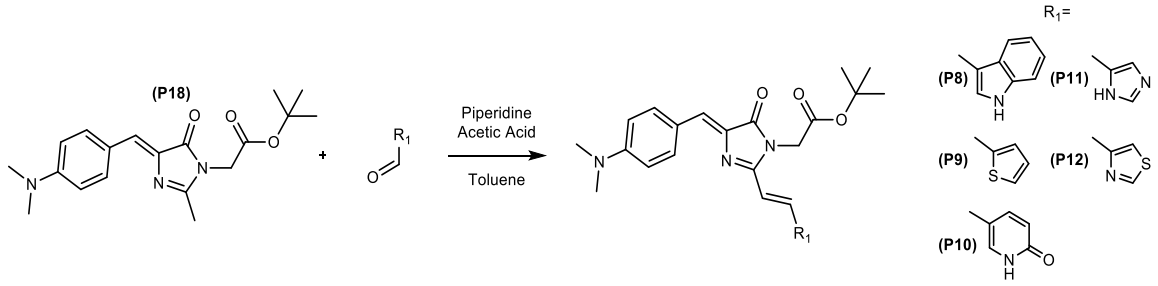

Scheme S4: Synthesis of P8-12

Conditions: aldehyde (1.5 mmol), P18 (343.0 mg, 1 mmol) were combine in toluene (2 mL) under Argon. Piperidine (824 µL, 8.0 mmol) and then acetic acid (458 µL, 8.0 mmol) were added and the reaction was refluxed at 110˚C overnight. Solvent was removed and was purified by flash chromatography (various conditions) to yield P8-P12**.**

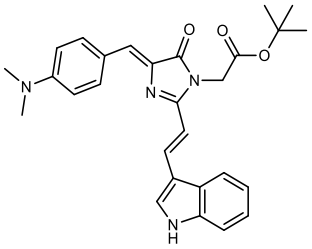

P8: Tert-butyl 2-(2-((E)-2-(1H-indol-3-yl)vinyl)-4-((Z)-4-(dimethylamino)benzylidene)-5-oxo-4,5-dihydro-1H-imidazol-1-yl)acetate. Red solid (25%).

^{1}H NMR (500 MHz, CDCl3) δ 8.49 (s, 1H), 8.27 (d, J = 15.6 Hz, 1H), 8.22 (d, J = 8.7 Hz, 1H), 7.99 – 7.90 (m, 1H), 7.80 – 7.74 (m, 2H), 7.55 (d, J = 34.1, 2.8 Hz, 1H), 7.46 (t, J = 7.2 Hz, 1H), 7.38 – 7.29 (m, 2H), 7.14 (s, 1H), 6.78 (d, J = 8.7 Hz, 1H), 6.73 (d, J = 8.9 Hz, 2H), 6.69 (d, 1H), 4.52 (s, 2H), 3.12 (s, 6H). ^{13}C NMR (126 MHz, CDCl3) δ 190.39, 154.35, 134.32, 128.48, 123.46, 121.52, 120.51, 111.91, 111.86, 111.00, 82.86, 42.34, 40.15, 40.12, 28.02. [M+H] Calcd, 471.2391; Obsd, 471.2391

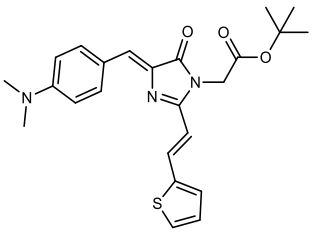

P9: Tert-butyl 2-(4-((Z)-4-(dimethylamino)benzylidene)-5-oxo-2-((E)-2-(thiophen-2-yl)vinyl)-4,5-dihydro-1H-imidazol-1-yl)acetate. Red solid (47%).

^{1}H NMR (500 MHz, $CDCl_3$) δ 8.19 (d, *J* = 8.6 Hz, 2H), 8.13 (d, *J* = 15.4 Hz, 1H), 7.38 (d, *J* = 5.0, 1.0 Hz, 1H), 7.31 (d, *J* = 3.6 Hz, 1H), 7.18 (s, 1H), 7.10 (dd, *J* = 5.1, 3.6 Hz, 1H), 6.77 (d, 2H), 6.43 (d, *J* = 15.5 Hz, 1H), 4.45 (s, 2H), 3.10 (s, 6H), 1.49 (s, 9H). ^{13}C NMR (126 MHz, $CDCl_3$) δ 170.06, 166.94, 155.30, 151.64, 141.18, 135.16, 134.67, 131.70, 130.10, 129.34, 128.26, 127.62, 122.89, 112.21, 111.84, 111.38, 82.96, 42.18, 40.11, 40.06, 29.72, 27.99 [M+H] Calcd, 438.1846; Obsd, 438.1844

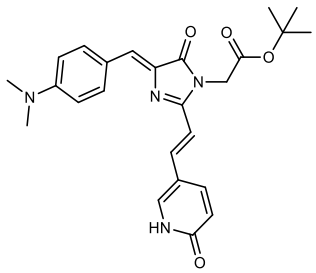

P10: Tert-butyl 2-(4-((Z)-4-(dimethylamino)benzylidene)-5-oxo-2-((E)-2-(6-oxo-1,6-dihydropyridin-3-yl)vinyl)-4,5-dihydro-1H-imidazol-1-yl)acetate. Red solid (17%)

^{1}H NMR (500 MHz, MeOD) δ 8.00 (d, 2H), 7.77 – 7.73 (m, 1H), 7.53 – 7.50 (m, 3H), 7.31 – 7.27 (m, 3H), 7.12 (s, 1H), 4.45 (s, 2H), 3.11 (s, 6H), 1.51 (s, 9H). ^{13}C NMR (126 MHz, MeOD) δ 190.98, 169.25, 167.13, 152.40, 134.64, 134.34, 130.11, 128.10, 121.19, 116.63, 111.58, 110.81, 102.62, 82.74, 82.54, 43.12, 41.72, 38.85, 38.76, 26.81, 26.78, 1.44. [M+H] Calcd, 449.2184; Obsd, 449.2182

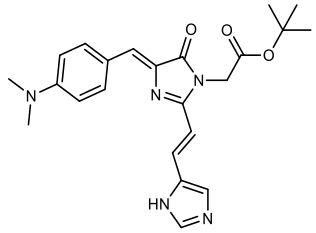

P11: Tert-butyl 2-(2-((E)-2-(1H-imidazol-5-yl)vinyl)-4-((Z)-4-(dimethylamino)benzylidene)-5-oxo-4,5-dihydro-1H-imidazol-1-yl)acetate. Red solid (19%).

^{1}H NMR (500 MHz, MeOD) δ 8.74 (s, 1H), 8.03 – 8.01 (m, 1H), 7.97 (d, 2H), 7.44 (s, 1H), 7.32 (d, *J* = 12.8 Hz, 1H), 7.01 (d, 2H), 6.49 (d, *J* = 12.8 Hz, 1H), 4.71 (s, 2H), 3.22 (s, 6H), 1.52 (s,

9H). ^{13}C NMR (126 MHz, CDCl3) δ 170.45, 167.04, 151.99, 151.50, 136.76, 135.22, 134.52, 133.79, 130.07, 128.63, 128.43, 122.95, 112.63, 112.01, 111.82, 111.58, 111.36, 111.01, 110.79, 110.67, 70.39, 67.11, 42.18, 40.17, 40.11, 40.06, 29.73, 28.17, 28.08. [M+H] Calcd, 422.2187; Obsd, 422.2183

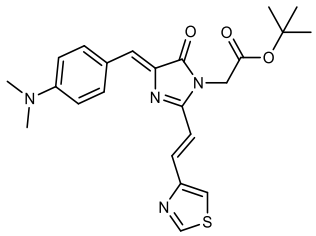

P12: Tert-butyl 2-(4-((Z)-4-(dimethylamino)benzylidene)-5-oxo-2-((E)-2-(thiazol-4-yl)vinyl)-4,5-dihydro-1H-imidazol-1-yl)acetate. Red solid (16%).

^{1}H NMR (500 MHz, $CDCl_3$) δ 8.87 – 8.85 (m, 1H), 8.20 (d, *J* = 8.6 Hz, 2H), 8.03 (d, *J* = 15.2 Hz, 1H), 7.50 (d, *J* = 1.9 Hz, 1H), 7.20 (s, 1H), 7.12 (d, *J* = 15.2 Hz, 1H), 6.77 – 6.75 (m, 2H), 4.47 (s, 2H), 3.10 (s, 6H), 1.47 (s, 9H). ^{13}C NMR (126 MHz, $CDCl_3$) δ 170.19, 166.87, 155.56, 153.65, 153.64, 153.51, 153.43, 152.60, 152.21, 151.68, 139.96, 135.16, 134.84, 134.76, 130.47, 129.78, 128.87, 125.40, 122.85, 122.39, 119.89, 115.95, 115.64, 111.81, 111.38, 82.93, 82.90, 53.47, 42.17, 42.14, 40.10, 40.06, 29.72, 28.00, 27.98. [M+H] Calcd, 439.1799; Obsd, 439.1797

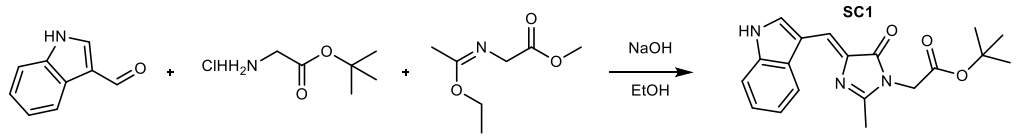

Scheme S5: Synthesis of Supplementary Compound 1 (**SC1**)

Conditions: glycine *tert*-butyl ester hydrochloride (183.7 mg, 1.1 mmol) was combine with NaOH (39.9 mg, 1 mmo1) in EtOH (2 mL) and stirred for 1 hr. at room temperature, indole-3-carboxaldehyde (145.1 mg, 1.0 mmol) was added and stirred overnight at 25˚C. Methyl (Z)-2-((1-ethoxyethylidene)amino)acetate (159 mg, 1.0 mmol) was prepared according to literature and added in one portion[11]. The reaction was stirred overnight at 25˚C, then quenched by water (5 mL) and extracted with ether (3x10 mL). The organic fraction was collected and dried in vacuo. Compounds were further purified by flash chromatography (66% Ethyl Acetate, 33% Hexanes) to yield **SC1** a yellow solid.

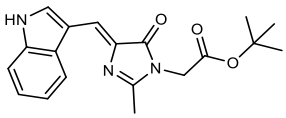

SC1: (Z)-tert-butyl 2-(4-((1H-indol-3-yl)methylene)-2-methyl-5-oxo-4, 5-dihydro-1H-imidazol-1-yl)acetate. Yellow powder (45%).

^{1}H NMR (500 MHz, DMSO-*d*6) 11.99 (s, 1H), 8.43 (d, *J*=2.8 Hz, 1H), 8.22 (d, *J*=7.7 Hz, 1H), 7.49 (d, *J*=7.9 Hz, 1H), 7.38 (s, 1H), 7.23 7.15 (m, 2H), 4.39 (s, 2H), 2.29 (s, 3H), 1.44 (s, 9H). *13*C NMR (126 MHz, DMSO-*d*6) 169.21, 167.94, 158.57, 136.90, 133.64, 127.18, 123.06, 121.30, 120.92, 120.18, 112.69, 111.56, 82.48, 42.31, 28.08, 15.54. [M+H] Calcd, 340.1583; Obsd, 340.1873

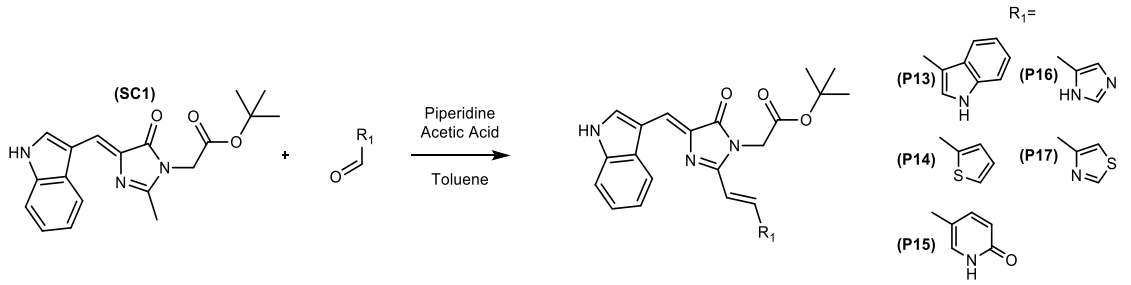

Scheme S6: Synthesis of P13-P17

Conditions: aldehyde (1.5 mmol), **SC1** (339.4 mg, 1 mmol) were combine in toluene (2 mL) under Argon. Piperidine (824 µL, 8.0 mmol) and then acetic acid (458 µL, 8.0 mmol) were added and the reaction was refluxed at 110˚C overnight. Solvent was removed and was purified by flash chromatography (various conditions) to yield P13-P17**.**

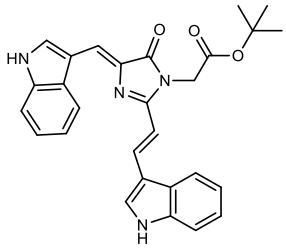

P13: Tert-butyl 2-((Z)-4-((1H-indol-3-yl)methylene)-2-((E)-2-(1H-indol-3-yl)vinyl)-5-oxo-4,5-dihydro-1H-imidazol-1-yl)acetate. Yellow-brown oil (20%).

^{1}H NMR (500 MHz, DMSO-d6) 12.02 (s, 1H), 11.84 (s, 1H), 8.60 (d, *J*=2.7 Hz, 1H), 8.27 (d, *J*=15.6 Hz, 1H), 8.20 (d, *J*=6.7 Hz, 1H), 8.08 7.96 (m, 2H), 7.59 7.46 (m, 2H), 7.34 (s, 1H), 7.31 7.16 (m, 4H), 6.76 (d, *J*=15.7 Hz, 1H), 4.65 (s, 2H), 1.42 (s, 9H). ^{13}C NMR (126 MHz, DMSO-d6) 168.04, 157.09, 137.99, 136.90, 133.32, 127.32, 125.32, 123.21, 123.09, 121.30, 120.69, 119.94, 118.39, 113.89, 112.99, 112.72, 82.43, 42.27, 28.11. [M+H] Calcd, 467.2078; Obsd, 467.2078

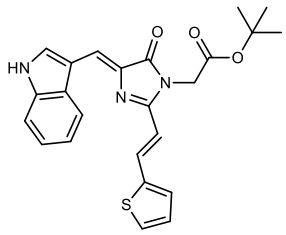

P14: Tert-butyl 2-((Z)-4-((1H-indol-3-yl)methylene)-5-oxo-2-((E)-2-(thiophen-2-yl)vinyl)-4,5-dihydro-1H-imidazol-1-yl)acetate. Orange oil (21%).

^{1}H NMR (500 MHz, $CDCl_3$) δ 8.79 (s, 1H), 8.68 (d, *J* = 2.8 Hz, 1H), 8.14 (d, *J* = 15.4 Hz, 1H), 8.06 – 8.00 (m, 1H), 7.65 (s, 1H), 7.47 – 7.44 (m, 1H), 7.40 (d, *J* = 5.0 Hz, 1H), 7.32 – 7.30 (m, 2H), 7.11 (dd, *J* = 5.0, 3.6 Hz, 1H), 6.44 (d, *J* = 15.4 Hz, 1H), 4.48 (s, 2H), 1.59 (s, 9H). ^{13}C NMR (126 MHz, $CDCl_3$) δ 169.37, 166.98, 155.33, 141.03, 135.92, 131.89, 130.21, 128.30, 127.82, 127.43, 123.36, 121.68, 121.12, 119.31, 113.25, 112.15, 111.59, 83.08, 53.45, 42.19, 29.73, 28.01, 14.15. [M+H] Calcd, 434.1533; Obsd, 434.1531

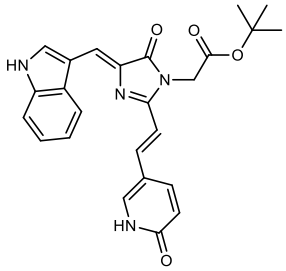

P15: Tert-butyl 2-((Z)-4-((1H-indol-3-yl)methylene)-5-oxo-2-((E)-2-(6-oxo-1,6-dihydropyridin-3-yl)vinyl)-4,5-dihydro-1H-imidazol-1-yl)acetate. Red oil (25%).

^{1}H NMR (500 MHz, $CDCl_3$) δ 9.62 (s, 1H), 9.31 (d, 1H), 8.96 (s, 1H), 8.71 (s, 1H), 8.37 – 8.32 (m, 1H), 7.90 (s, 1H), 7.86 (d, *J* = 2.9 Hz, 1H), 7.69 (s, 1H), 7.46 (d, *J* = 5.8 Hz, 2H), 7.34 (d, *J* = 8.9 Hz, 2H), 4.38 (s, 2H), 1.51 (s, 9H). ^{13}C NMR (126 MHz, CDCl3) δ 192.94, 185.21, 171.24, 167.09, 150.46, 150.09, 132.62, 132.15, 130.25, 130.00, 129.86, 129.45, 126.85, 126.49, 125.89, 124.46, 124.26, 123.32, 122.92, 122.34, 121.92, 121.56, 121.00, 111.94, 111.67, 90.79, 83.14, 70.19, 67.10, 66.15, 62.43, 60.44, 55.21, 53.46, 41.94, 29.72, 28.51, 28.21, 28.11, 28.02, 27.99, 27.69, 27.41, 21.09, 14.22. [M+H] Calcd, 445.1831; Obsd, 445.1868

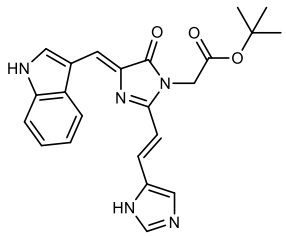

P16: Tert-butyl 2-((Z)-2-((E)-2-(1H-imidazol-5-yl)vinyl)-4-((1H-indol-3-yl)methylene)-5-oxo-4,5-dihydro-1H-imidazol-1-yl)acetate. Orange Solid (10%).

^{1}H NMR (500 MHz, $CDCl_3$) δ 8.67 (s, 1H), 8.36 – 8.29 (m, 1H), 8.20 (d, *J* = 15.6 Hz, 1H), 8.10 – 8.03 (m, 2H), 7.92 – 7.86 (m, 2H), 7.80 (d, *J* = 1.9 Hz, 1H), 7.59 (d, *J* = 14.7 Hz, 1H), 7.41 – 7.40 (m, 1H), 7.31 – 7.30 (m, 1H), 6.61 (d, *J* = 15.7 Hz, 1H), 4.54 (s, 2H), 1.52 (s, 9H). ^{13}C NMR (126 MHz, $CDCl_3$) δ 172.28, 167.19, 150.93, 141.69, 137.94, 135.79, 130.69, 129.35, 129.00, 127.66, 123.96, 122.36, 122.04, 118.16, 114.39, 113.14, 110.01, 109.70, 82.02, 44.09, 28.09. [M-H] Calcd, 416.1728; Obsd, 416.2095

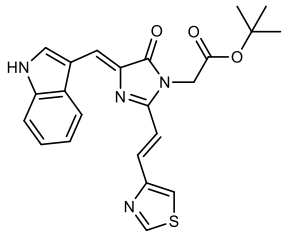

P17: Tert-butyl 2-((Z)-4-((1H-indol-3-yl)methylene)-5-oxo-2-((E)-2-(thiazol-4-yl)vinyl)-4,5-dihydro-1H-imidazol-1-yl)acetate. Orange Solid (10%).

^{1}H NMR (500 MHz, $CDCl_3$) δ 9.11 (s, 1H), 8.79 (d, 1H), 7.64 – 7.53 (m, 2H), 7.38 (d, J = 8.6 Hz, 2H), 7.29 (d, J = 13.7 Hz, 1H), 7.23 (m, 1H), 7.07 (m, 1H), 6.95 (d, J = 13.7 Hz, 1H), 6.88 (s, 1H), 4.45 (s, 2H) 1.50 (s, 9H). ^{13}C NMR (126 MHz, $CDCl_3$) δ 172.28, 167.19, 150.93, 141.69, 137.94, 135.79, 130.69, 129.35, 129.00, 127.66, 123.96, 122.36, 122.04, 118.16, 114.39, 113.14, 110.01, 109.70, 82.02, 44.09, 28.09. [M+H] Calcd, 435.1486; Obsd, 435.1446

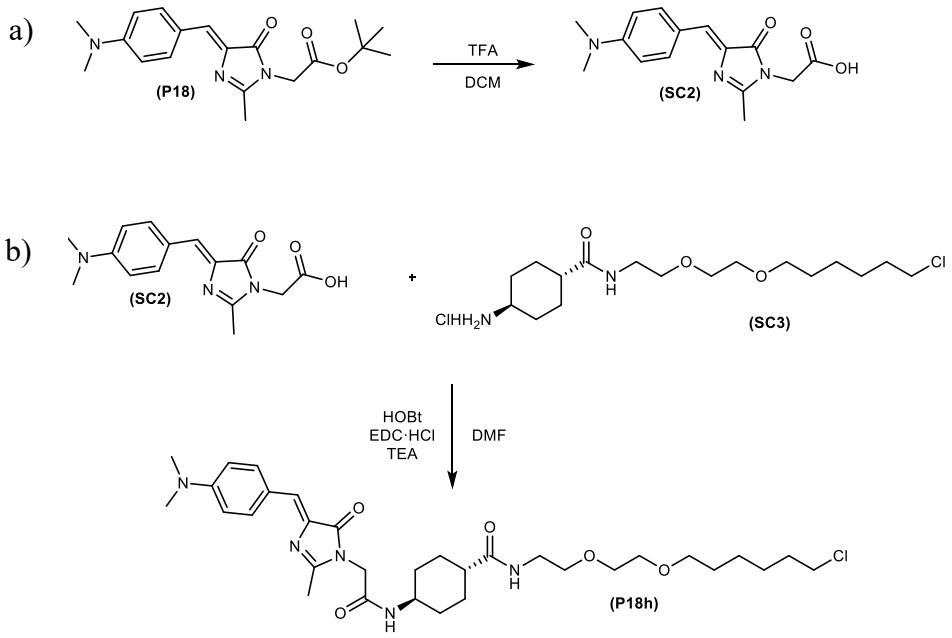

Scheme S7: Synthesis of P18h

Conditions: a) P18 (343.9 mg, 1.0 mmol) was deprotected according to standard protocols with trifluoracetic acid (1.5 mL, 20 mmol) in dichloromethane (5 mL) for 1 hr. at 25˚C and monitored via TCL (50% Ethyl Acetate/50% Hexanes) to yield **SC2,** which was used without further purification.

Conditions: b) **SC3** was prepared according to pervious literature protocols[12]. **SC2** (287.1 mg, 1.0 mmol), **SC3** (384.1 mg, 1.0 mmol), 1-Hydroxybenzotriazole hydrate (270.2 mg, 2.0 mmol), N-(3-Dimethylaminopropyl)-N′-ethylcarbodiimide hydrochloride (287.6 mg, 1.5 mmol), and triethylamine (836 mg, 6.0 mmol) were combined in DMF (10 mL) and stirred overnight at 25˚C. The reaction mixture was quenched by water (5 mL) and extracted with DCM (3x10 mL). The organic fraction was collected and dried in vacuo. Crude mixture was purified by flash chromatography (100% Ethyl Acetate) to yield P18h a yellow powder.

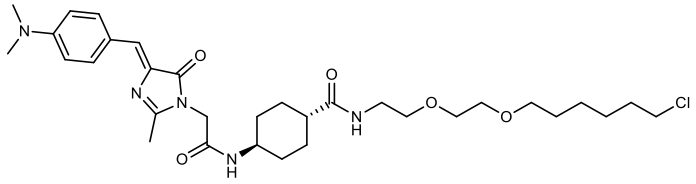

P18h: (1r,4r)-N-(2-(2-((6-chlorohexyl)oxy)ethoxy)ethyl)-4-(2-((Z)-4-(4-(dimethylamino)benzylidene)-2-methyl-5-oxo-4,5-dihydro-1H-imidazol-1-yl)acetamido)cyclohexanecarboxamide. Yellow powder (51%).

^{1}H NMR (500 MHz, Chloroform-*d*) δ 8.09 (d, *J* = 8.8 Hz, 2H), 7.14 (s, 1H), 6.73 (d, *J* = 8.9 Hz, 2H), 6.17 – 5.87 (m, 2H), 4.23 (s, 2H), 3.60 – 3.40 (m, 12H), 3.09 (s, 6H), 2.40 (s, 3H), 2.10 – 1.18 (m, 16H), 1.22 – 1.09 (m, 2H). ^{13}C NMR (126 MHz, Chloroform-d) δ 175.00, 170.58, 166.30, 157.55, 151.89, 134.59, 133.56, 130.57, 121.84, 111.77, 71.27, 70.24, 70.00, 69.81, 48.21, 45.08, 44.76, 44.37, 40.05, 39.02, 32.52, 32.03, 29.46, 28.26, 26.69, 25.41, 15.59. [M+H] Calcd, 618.3344; Obsd, 618.3441.

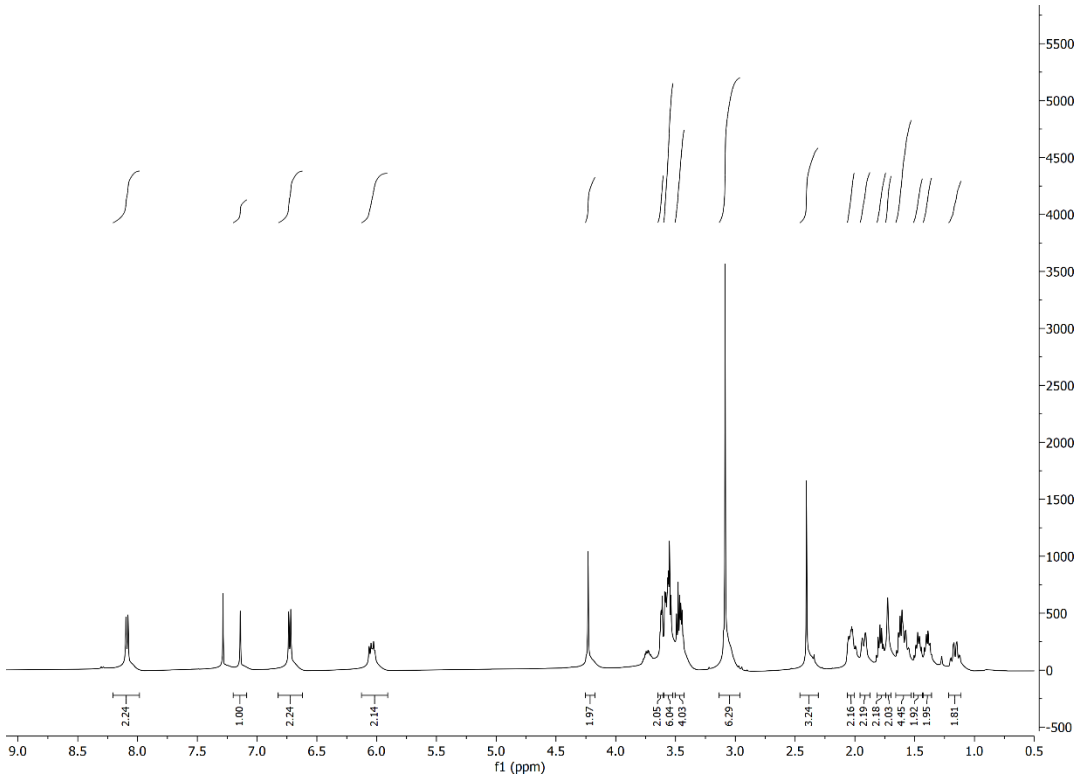
2.24
1.00
2.24
2.14
1.97
2.05
6.04
4.03
6.29
3.24
2.16
2.19
2.18
2.03
4.45
1.92
1.95
1.81
f1 (ppm)

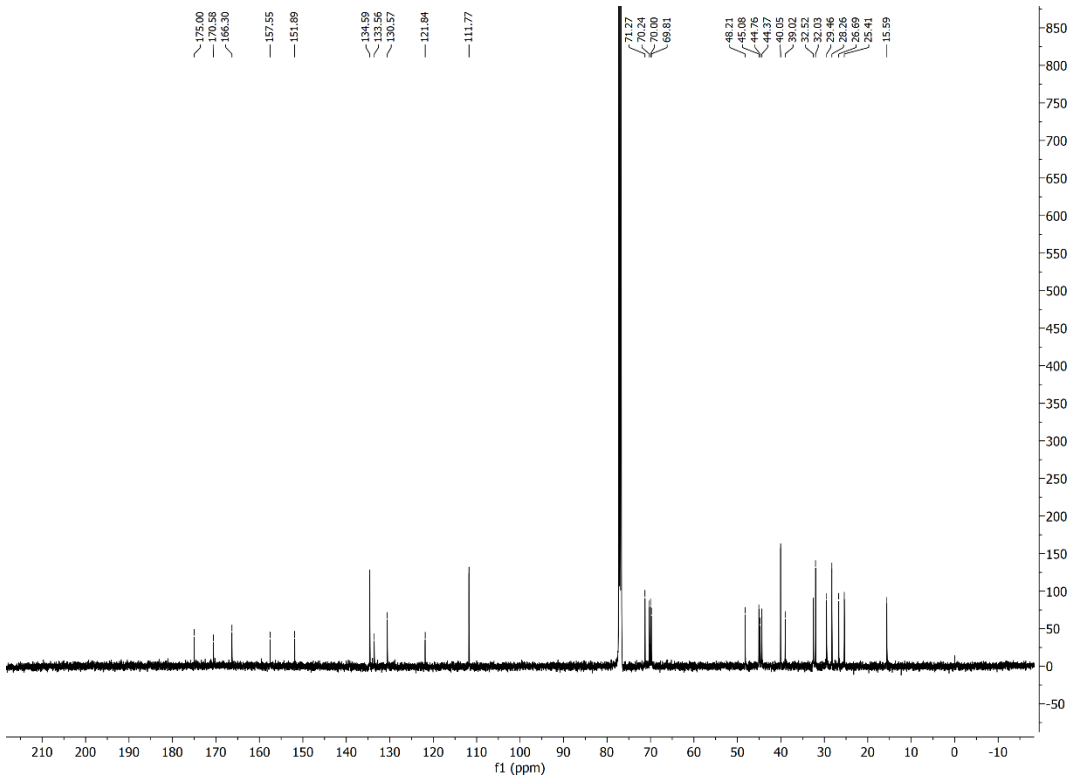
175.00
170.58
166.30
157.55
151.89
134.59
133.56
130.57
121.84
111.77
71.27
70.24
70.00
69.81
48.21
45.08
44.76
44.37
40.05
39.02
32.52
32.03
29.46
28.26
26.69
25.41
15.59
f1 (ppm)

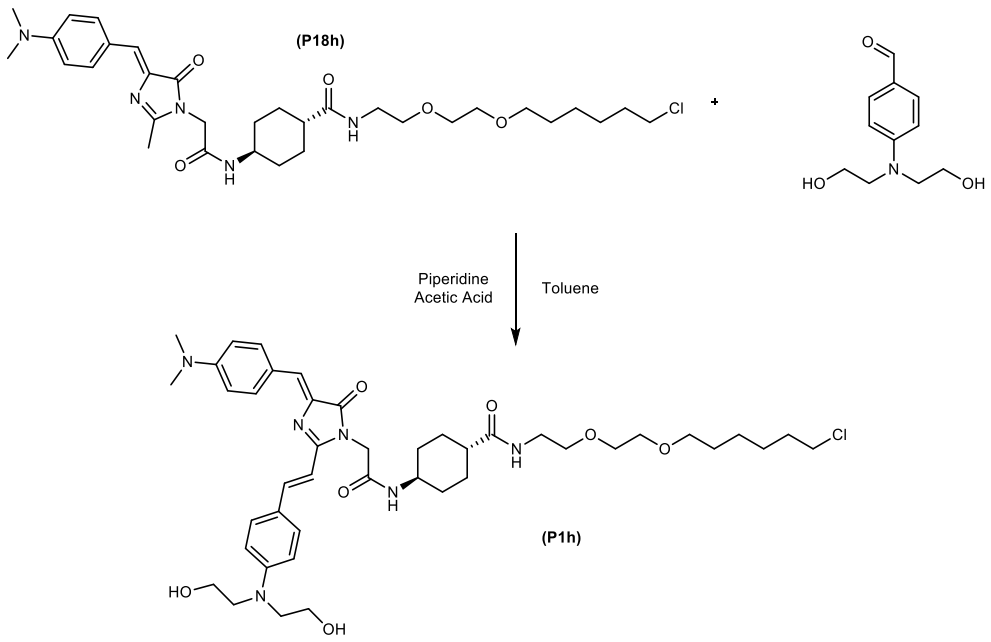

Scheme S8: Synthesis of P1h

Condition: 4-[Bis(2-hydroxyethyl)amino]benzaldehyde (313.6 mg, 1.5 mmol), P18h (602.3 mg, 1.0 mmol) were combine in toluene (5 mL) under Argon. Piperidine (824 µL, 8.0 mmol) and then acetic acid (458 µL, 8.0 mmol) were added and the reaction was refluxed at 110˚C overnight. Solvent was removed and crude mixture was purified by flash chromatography (5% MeOH, 95% DMC) to yield P1h a red oil.

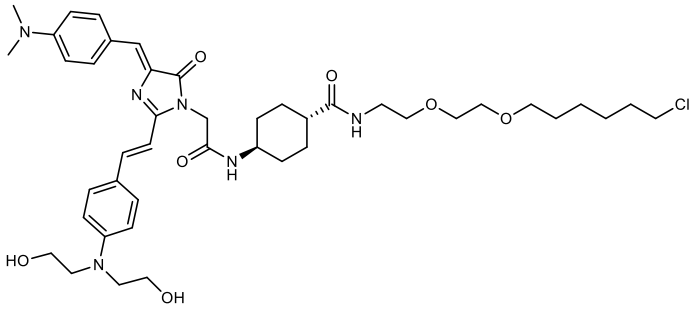

P1h: 4-(2-((E)-2-((E)-4-(bis(2-hydroxyethyl)amino)styryl)-4-(4-(dimethylamino)benzylidene)-5-oxo-4,5-dihydro-1H-imidazol-1-yl)acetamido)-N-(2-(2-((6-chlorohexyl)oxy)ethoxy)ethyl)cyclohexanecarboxamide. Red solid (20%).

^{1}H NMR (500 MHz, DMSO-d6) δ 8.17 (d, J = 8.3 Hz, 2H), 7.79 (d, J = 15.5 Hz, 1H), 7.55 (d, J = 8.7 Hz, 2H), 6.84 (s, 1H), 6.80 (d, J = 9.9, 2.7 Hz, 2H), 6.75 (d, J = 8.6, 5.5 Hz, 2H), 6.66 (d, J = 15.5 Hz, 1H), 4.82 (m, 2H), 4.38 (s, 2H), 3.64 – 3.55 (m, 8H), 3.54 – 3.43 (m, 8H), 3.40-3.36 (m, 4H), 3.22-3.12 (m, 2H), 3.04 (s, 6H), 1.86-1.81 (m, 2H), 1.75-1.66 (m, 4H), 1.53-1.45 (m, 2H), 1.43 – 1.17 (m, 10H). ^{13}C NMR (126 MHz, DMSO-d6) δ 175.25, 170.23, 166.41, 158.08, 151.50, 150.03, 136.00, 134.27, 130.24, 122.98, 122.85, 112.29, 111.90, 70.64, 70.05, 69.90, 69.56, 58.61, 58.44, 53.60, 48.10, 45.84, 43.53, 38.85, 32.49, 32.08, 29.54, 28.61, 26.59, 25.40. [M+H] Calcd, 809.4357; Obsd, 809.4369

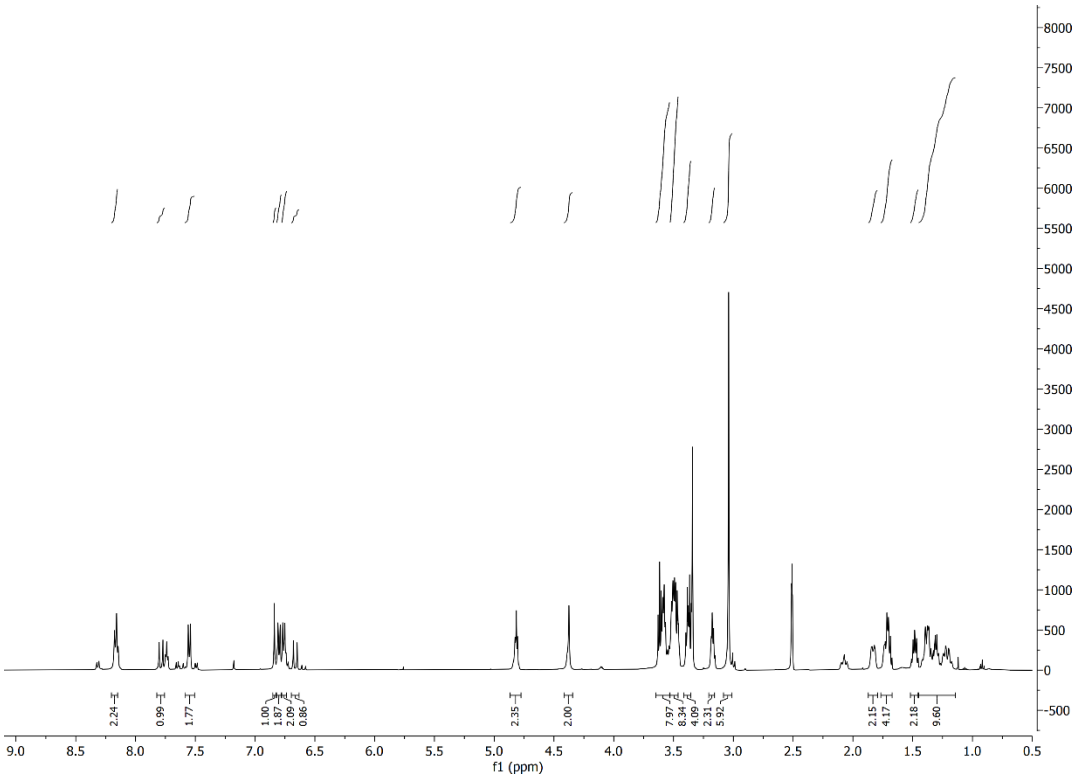
2.24
0.99
1.77
1.00
1.87
2.09
0.86
2.35
2.00
7.97
8.34
4.09
2.31
5.92
2.15
4.17
2.18
9.60
f1 (ppm)

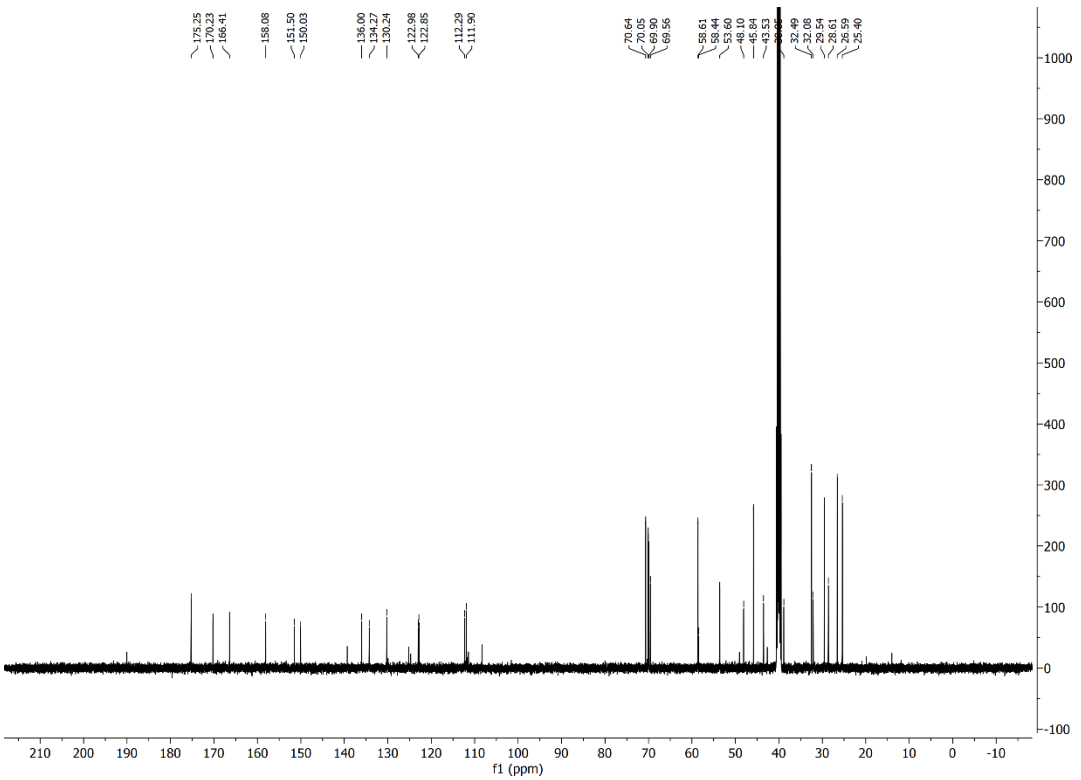
175.25
170.23
166.41
158.08
151.50
150.03
136.00
134.27
130.24
122.98
122.85
112.29
111.90
70.64
70.05
69.90
69.56
58.61
58.44
53.60
48.10
45.84
43.53
40.66
32.49
32.08
29.54
28.61
26.59
25.40
f1 (ppm)

6. Supplementary Notes

Note S1. Temperature-independence of P1 and P18 Fluorescent Emission

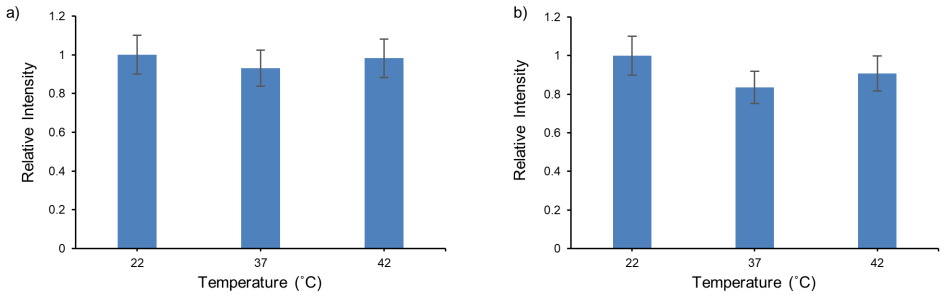

Emission spectrum for P1 (**a**) and P18 (**b**) were recorded in water and glycerol mixtures at varying temperatures. All samples exhibit similar viscosity (cp) values: 22 ˚C - 89.5% glycerol (243 cp), 37 ˚C – 97.5% glycerol (243 cp) and 42 ˚C – 100% glycerol (245 cp). All fluorophores were dissolved with a final concentration at 5 μM and excited at 540 nm for P1 and 450 nm for P18 using a Tecan infinite M1000Pro fluorescence microplate reader with temperature control function. Fluorescence emission intensity of both probes were independent of temperatures of 22, 37, and 42ºC.

Note S2. Beer-Lambert Plots of P2-P17

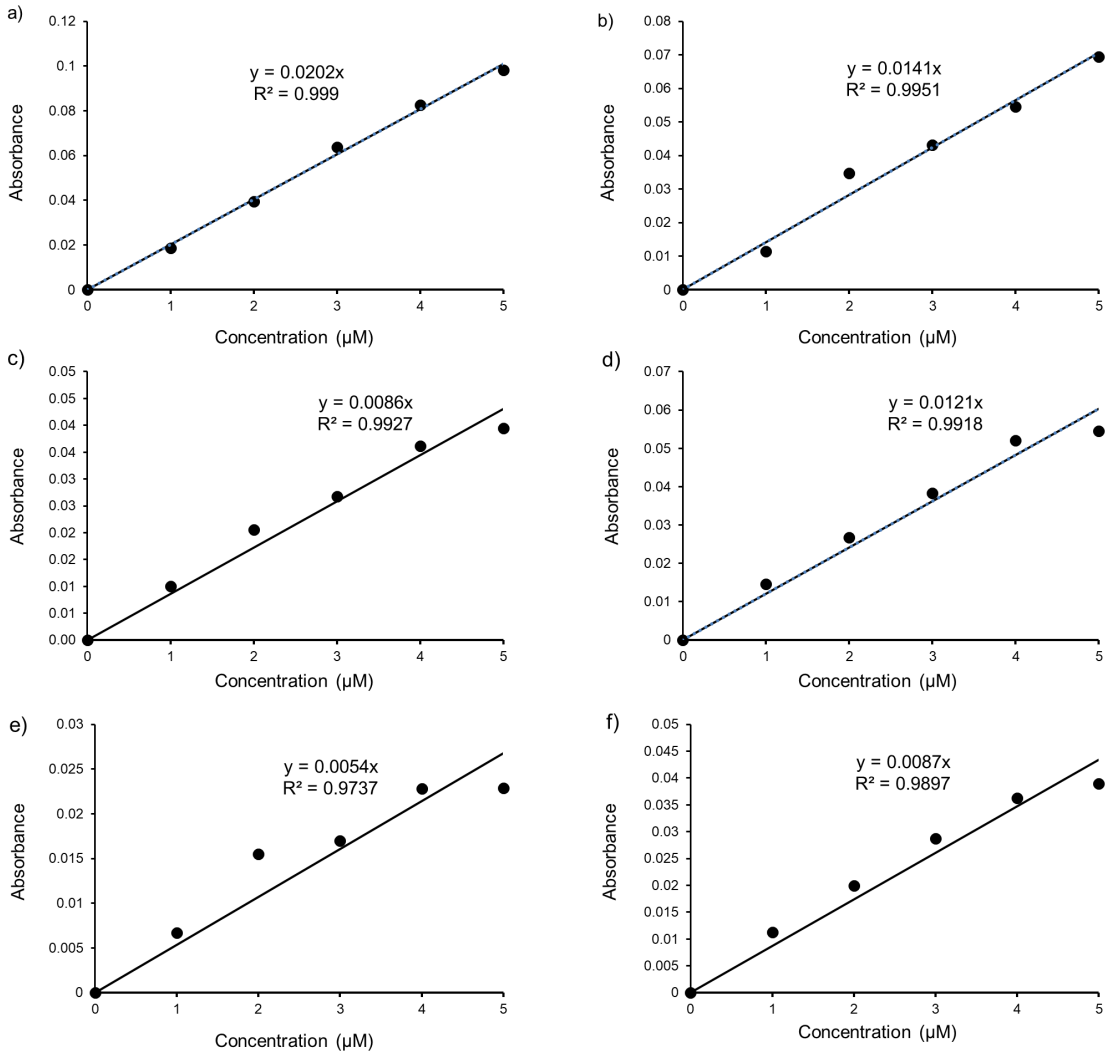

Plot of absorbance at λ_{max} as a function of concentration for P2-7: **a**) P2, **b**) P3, **c**) P4, **d**) P5, **e**) P6, **f**) P7. All fluorophores were dissolved in glycerol with a final concentration of 1-5 μM and absorption peak was measured using a Tecan infinite M1000Pro fluorescence microplate reader. The linear relationship in this concentration range shows the probes are not undergoing self-induced aggregation.

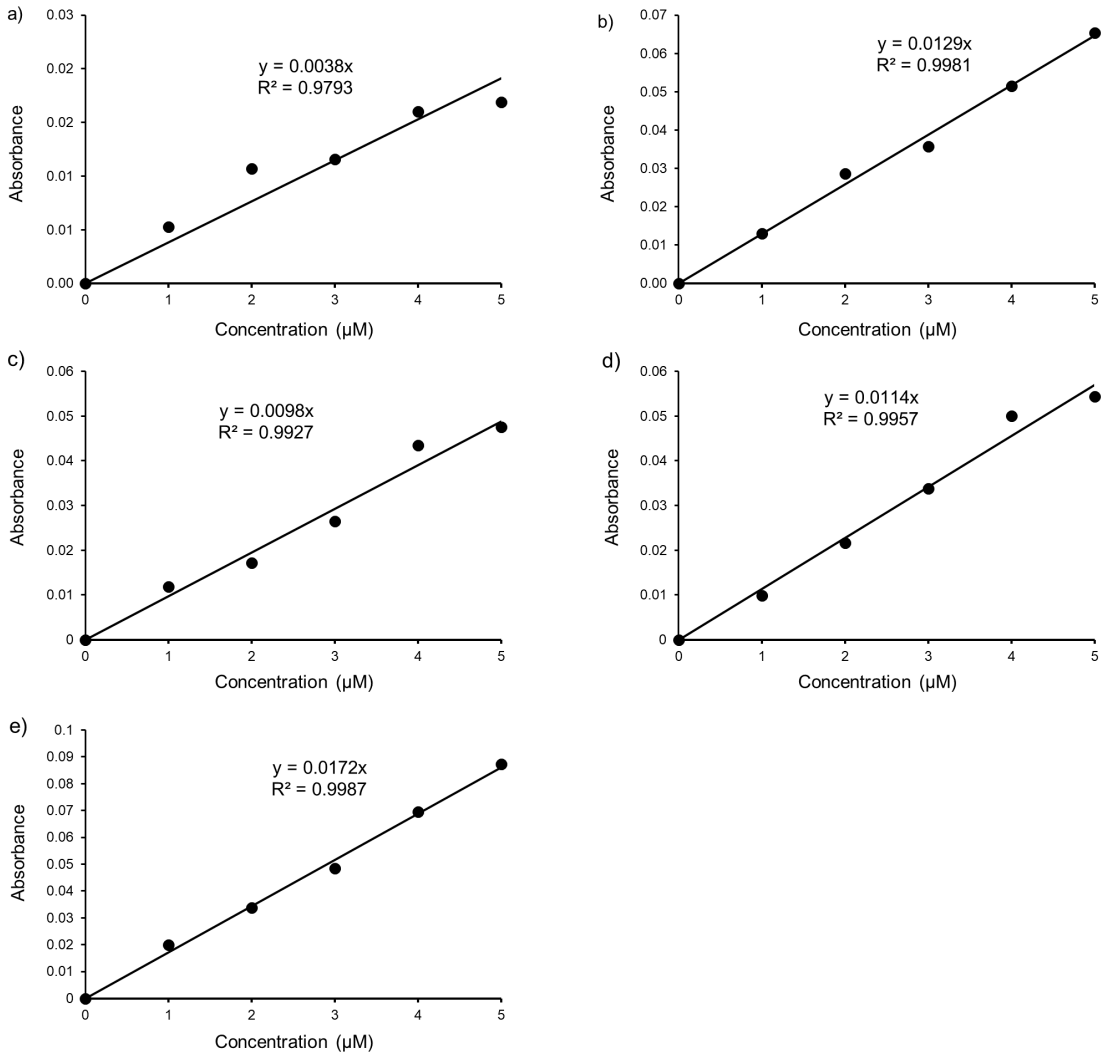

Plot of absorbance at λ_{max} as a function of concentration for P8-11: **a**) P8, **b**) P9, **c**) P10, **d**) P11, **e**) P12. All fluorophores were dissolved in glycerol with a final concentration of 1-5 μM and absorption peak was measured using a Tecan infinite M1000Pro fluorescence microplate reader. The linear relationship in this concentration range shows the probes are not undergoing self-induced aggregation.

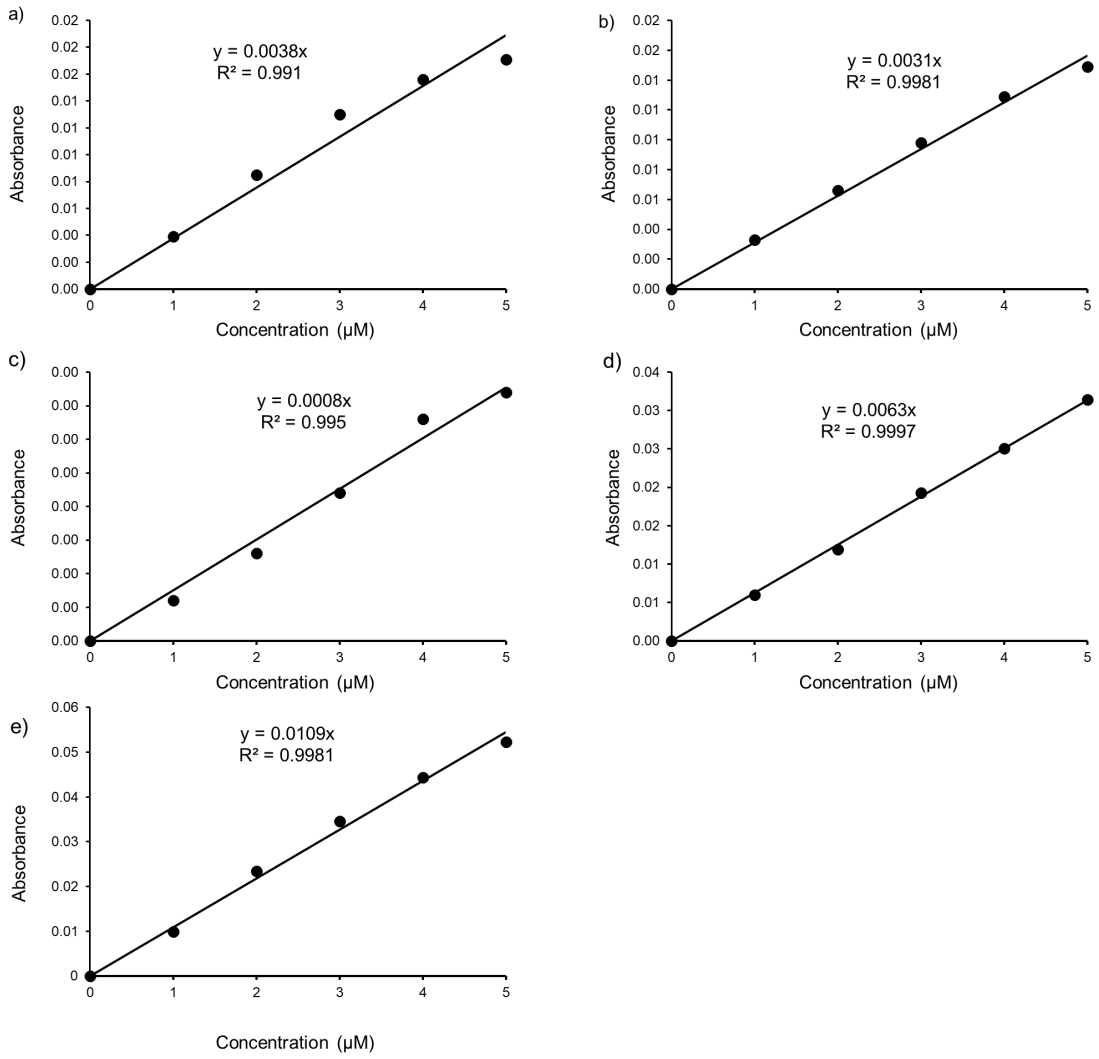

Plot of absorbance at λ_{max} as a function of concentration for P13-17: **a**) P13, **b**) P14, **c**) P15, **d**) P16, **e**) P17. All fluorophores were dissolved in glycerol with a final concentration of 1-5 μM and absorption peak was measured using a Tecan infinite M1000Pro fluorescence microplate reader. The linear relationship in this concentration range shows the probes are not undergoing self-induced aggregation.

Note S3. Limit of Detection for P1h and P18h

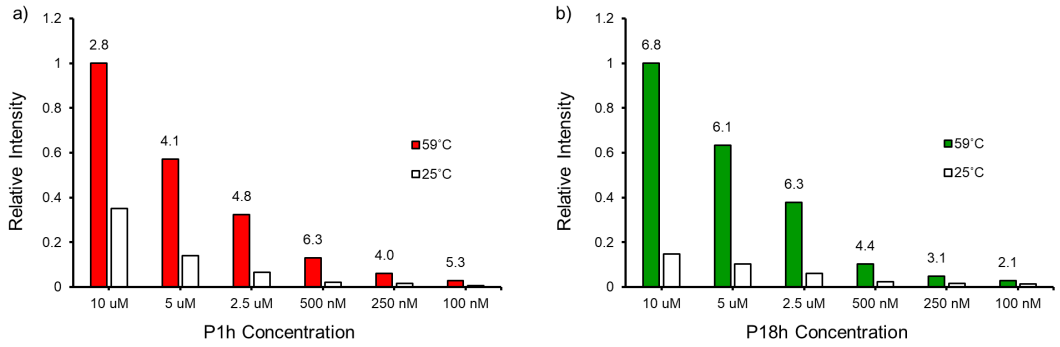

LOD refers to the lower limit amount of protein aggregates that the probe could detect. Essentially, the LOD is determined by whether the signal-to-noise ratio is sufficient at low concentrations of either protein aggregates or probes. Thus, we designed an experiment wherein the probe concentrations vary between 0.1 μM and 10 μM, when conjugated to 25 μM of purified SOD1(A4V)-Halo (similar experiment to Figure 5d). The signal is defined as fluorescence intensity when P1h or P18h are detecting protein aggregates (59 ºC that induced aggregation of SOD1-A4V-Halo) and the noise is defined as fluorescence intensity when P1h or P18h conjugated with folded proteins (25 ºC wherein SOD1-A4V-Halo is folded). For P1h, our results show that concentrations between 0.1 to 5 μM yields the best fluorescence increase (4-6 fold) induced by protein aggregation. For P18h, this range is between 0.5 to 10 μM (4-7 fold). Thus, we conclude that the LOD for P1h is 0.1 μM and P18h is 0.5 μM. In our applications, the in vitro experiment used 5 μM and cellular imaging experiment used 0.5 μM, both of which are within the range of effective concentrations of P1h and P18h. Aggregation of SOD1-(A4V)-Halo was carried out with DPBS buffer with 80 mM EDTA added after conjugation to chelate the structural metal. Conjugation of P1h or P18h to purified SOD1-(A4V)-Halo protein was completed by incubation of the probe (various concentrations) with protein (25 μM) in a 1.5 mL microcentrifuge tube for 15 min in the absence of ambient light prior. Reaction was carried out quiescently at indicated temperatures for 25 minutes. Emission spectrum for P1h (**a**) and P18h (**b**) were recorded using a Tecan infinite M1000Pro fluorescence microplate reader.

7. References

1 Wurth, C., Grabolle, M., Pauli, J., Spieles, M. & Resch-Genger, U. Relative and absolute determination of fluorescence quantum yields of transparent samples. *Nat Protoc* **8**, 1535-1550, (2013).

2 Zhang, X. *et al.* The Heat-Shock Response Transcriptional Program Enables High-Yield and High-Quality Recombinant Protein Production in Escherichia coli. *ACS Chem Biol* **9**, 1945-1949 (2014).

3 Olsen, S. & Smith, S. C. Radiationless decay of red fluorescent protein chromophore models via twisted intramolecular charge-transfer states. *J Am Chem Soc* **129**, 2054-2065, (2007).

4 Eade, R. H. A. & Robb, M. A. Direct Minimization in Mc Scf Theory - the Quasi-Newton Method. *Chem Phys Lett* **83**, 362-368, (1981).

5 Bochenkova, A. V. & Andersen, L. H. Ultrafast dual photoresponse of isolated biological chromophores: link to the photoinduced mode-specific non-adiabatic dynamics in proteins. *Faraday Discuss* **163**, 297-319, (2013).

6 Paolino, M. *et al.* Design, Synthesis, and Dynamics of a Green Fluorescent Protein Fluorophore Mimic with an Ultrafast Switching Function. *J Am Chem Soc* **138**, 9807-9825, (2016).

7 Martin, M. E., Negri, F. & Olivucci, M. Origin, nature, and fate of the fluorescent state of the green fluorescent protein chromophore at the CASPT2//CASSCF resolution. *J Am Chem Soc* **126**, 5452-5464, (2004).

8 Polyakov, I., Epifanovsky, E., Grigorenko, B., Krylov, A. I. & Nemukhin, A. Quantum Chemical Benchmark Studies of the Electronic Properties of the Green Fluorescent Protein Chromophore: 2. Cis-Trans Isomerization in Water. *J Chem Theory Comput* **5**, 1907-1914, (2009).

9 Frisch, M. J., Pople, J. A. & Binkley, J. S. Self-Consistent Molecular-Orbital Methods .25. Supplementary Functions for Gaussian-Basis Sets. *J Chem Phys* **80**, 3265-3269, (1984).

10 Becke, A. D. Density-Functional Thermochemistry .3. The Role of Exact Exchange. *J Chem Phys* **98**, 5648-5652, (1993).

11 Baldridge, A., Kowalik, J. & Tolbert, L. M. Efficient Synthesis of New 4-Arylideneimidazolin-5-ones Related to the GFP Chromophore by 2+3 Cyclocondensation of Arylideneimines with Imidate Ylides. *Synthesis-Stuttgart*, 2424-2436, (2010).

12 Liu, Y. *et al.* Modulation of Fluorescent Protein Chromophores To Detect Protein Aggregation with Turn-On Fluorescence. *J Am Chem Soc* **140**, 7381-7384, (2018).